UNIVERSIDADE DE SÃO PAULO
INSTITUTO DE GEOCIÊNCIAS

MICROSTRUCTURAL, THERMOMETRIC AND VORTICITY ANALYSIS OF MYLONITIC ROCKS FROM THE WESTERN SECTOR OF TAXAQUARA SHEAR ZONE (PILAR DO SUL, SP)

Bruno Vieira Ribeiro

Orientador: Prof. Dr. Ginaldo Ademar da Cruz Campanha
Co – Orientador: Prof. Dr. Frederico Meira Faleiros

MONOGRAFIA DE TRABALHO DE FORMATURA
(TF - 2017/ 06)

SÃO PAULO
2017

“O sorriso que tenho nos lábios
é um sorriso geológico – o sorriso
de quem sabe, olha, vê e compreende”
Monteiro Lobato

“Learn from yesterday, live for today, hope for tomorrow.
The important thing is not to stop questioning.”
Albert Einstein

AGRADECIMENTOS

Antes de tudo, gostaria de agradecer todo o apoio dos meus pais que, frente às diversas dificuldades passadas, nunca deixaram de me apoiar até mesmo nas minhas decisões mais loucas, por mais que não concordassem. Deixaram eu tomá-las e, por mim mesmo, ver o que era o melhor ou não para mim. Não tenho palavras para descrever e agradecer tudo o que vocês fizeram e fazem por mim. O suporte de vocês me fez chegar até aqui e, sem dúvidas, me levará muito longe! Como costumamos dizer, “ao infinito e além”. Amo vocês!

Muito tenho a agradecer aos Professores Ginaldo Campanha e Frederico Faleiros que me orientaram nesses últimos anos de faculdade culminando neste Trabalho de Formatura. Muito obrigado por toda a ajuda, suporte, conversas, sugestões e discussões acadêmicas que tivemos nesse tempo (e estou certo de que essa parceria será estendida). Além disso, agradeço aos relatores deste trabalho, Professor Carlos Archanjo e Professora Lucelene Martins, pelos comentários a fim de elevar a qualidade da monografia.

Agradeço imensamente ao Professor Roberto Weinberg pela oportunidade de estágio no exterior na *Monash University* para realização de parte desta monografia. Sua contribuição foi de suma importância e ter contato com uma pessoa como você, apaixonado pelo que faz e pela ciência, foi inspirador.

Outra pessoa que gostaria de agradecer nominalmente é a Professora Adriana Alves. Adri, foi você que despertou em mim o desejo pela ciência e pela busca do conhecimento. Foi você quem me ensinou as pequenas coisas, porém muito importantes: escrever um relatório, avaliar os dados e o que fazer com eles e a superar as frustrações. Se hoje almejo me tornar um cientista e professor, saiba que você é uma das minhas maiores inspirações e serei eternamente grato por tudo que fizemos juntos (e que ainda poderemos fazer!). Me desculpe por nem sempre ser o aluno que você merecia, mas dei meu melhor! E obrigado por todas as conversas pessoais.

Agradeço de coração todos os professores e professoras que lecionaram alguma disciplina para mim e minha turma. Nominalmente, agradeço aos Professores Rogério Azzone, Fabio Ramos, PC Giannini, Colombo Tassinari, Excelso Ruberti, Marcos Egydio, Mario Campos, Miguel Basei, Wilson Teixeira, Maria Helena, Renato de Moraes, André Negrão, Caetano Juliani, Lena Monteiro, Marcelo Monteiro e Renato Paes de Almeida. Muito obrigado por todos esses anos.

Confesso que ao longo desses seis anos, fui sempre muito bem acompanhado nos momentos de estudo e desespero pré provas, de cervejas (no CEPEGE, nos campos, nas festas, nos bares, no BIFE), de baladas, de bad trip entre outras infinitas situações. Foi durante a faculdade que fiz grandes amigos e amigas que, tenho certeza, ficarão mesmo após esse momento de transição que é sempre difícil. Chega a ser difícil ter palavras para agradecer todos os momentos que passamos juntos, todas as loucuras que fizemos, toda a história que construímos (calma que ainda tem BIFE 2017!). Nominalmente, quero muito agradecer meus amigos e amigas Vitor Malagutti (Tênia), Lys Plantullo (Shirley), Raul Beber (Vera), Luigi Carboni (Sinoca), Vitor Sette (Pedritinha), Bruno Consentino (Constilok), Everton (Manja), Lorena Guering (Free), Aline Ansara (Dama), Gabriel Rangel (Huguera), Lucas Milani, Tania

Cruz, Gabi Bazilli (Vads), Lourenço (Mediocre), Igor Barboza (Titchon), Bruna Ricardo (Gari), Carol Paes (Peps), Fernando Bergamini, João Mariante (Bug), José Guilherme, Paulo Koki (Pika), Lorenzo Calabria (Moleston), Felipe Silva (Lelek), Ivan Pantaleoni (Pinkzera), Wesley de Souza, Guilherme Fernandez (Piri). Tamo junto, malandragem! Se esqueci de alguém, desculpas desde já!

Muito tenho a agradecer ao Vôlei da Geo-USP que comecei a participar em 2012 e, desde então, tem me dado muita alegria. Através do vôlei conheci muita gente legal da Geo e da USP, fiz bons amigos e amigas, jogamos muitos campeonatos (embora sem grandes vitórias), outros tantos amistosos (com algumas boas vitórias) e bebemos várias cervejinhas. Agradeço muito a todos com quem eu pude jogar durante esses anos e a todos aqueles que me ajudaram a evoluir tecnicamente no esporte. Muito obrigado por ter me apresentado pessoas incríveis de outras faculdades e por todos os BIFEs. Amo vocês!

Agradeço a todos os funcionários da Geologia que mantém a faculdade em ordem, aos motoristas que nos levam para cima e para baixo, aos técnicos e técnicas dos laboratórios e todos aqueles nos auxiliam em tudo que for necessário.

Por fim, mas não menos importante, agradeço imensamente o pessoal do “Matemática em Movimento”. Por anos, participar de uma ONG como a nossa foi a minha válvula de escape. Foi com vocês que mais evolui, tanto pessoal quanto profissionalmente. Vocês são uma fonte de inspiração para mim e nunca me esquecerei de tudo que vivemos, das dificuldades e das conquistas. Aqui não vou agradecer nominalmente porque seriam muitas pessoas, mas não posso deixar de agradecer ao Rafa Rabioglio e Tiago Tenuto por todo o suporte e ensinamentos nesse tempo todo (e até hoje!). Eu amo vocês todos.

Este trabalho foi realizado com apoio financeiro das agências de fomento FAPESP (Proc. 2016/22051-4, 2017/08919-4 para Bruno Ribeiro e 2015/04487-7 para Frederico Faleiros) e CNPq (Proc. 443439/20141 and 305074/2015-6 para Ginaldo Campanha).

ABSTRACT

The NE-trending dextral Taxaquara Shear Zone (TSZ) is a major strike-slip structure within the Neoproterozoic Ribeira Belt (SE Brazil) developed during Late Ediacaran to Cambrian related to the Brazilian-Pan African Orogeny. The TSZ structure was investigated in its southwestern region using field, microstructural, CPO and vorticity analysis in order to infer T, stress flow, strain rate, viscosity and deformation conditions. It is characterized by a mylonitic foliation (N062E/70SE) with a sub-horizontal to oblique plunging stretching lineation. The analyzed rocks are intensely deformed orthoderivated mylonites with a mineral assemblage that reflects deformation at upper greenschist facies in the stability field of biotite and epidote with a matrix composed of quartz + feldspar + biotite + muscovite ± epidote). Subgrain rotation (SGR) is the main mechanism of dynamic recrystallization for quartz with minor contribution of grain boundary migration (GBM). Feldspar porphyroclasts record brittle (microfaults) and ductile deformation (BLG and SGR) forming clasts surrounded by well-developed fine-coursed mantle of recrystallization. The samples yield a narrow range of vorticity number using the rigid porphyroclasts method ($W^{RP}_m \approx 0.43$-0.70) suggesting shearing under moderate to high strain conditions. Results from δ/β-method demonstrate variation between pure ($W^{\delta/\beta}_m \approx 0.24$-$0.47$) and simple shear ($W^{\delta/\beta}_m \approx 0.85$-$0.99$) along the strike of TSZ, which is also demonstrated through quartz CPO geometries varying from monoclinic to orthorhombic. These data agree with the inference from regional geology for a transpressional system but with prevalence of simple shear over pure shear in the studied area. Quartz CPO displays contribution of ‘basal-<a>’ and ‘rhomb-<a>’ slip system for samples from the NE sector of the shear zone, whereas ‘rhomb-<a>’ and ‘prism-<a>’ are predominant in samples from a region 3 km to SW. Combined, the data indicate mylonitization in the deformation temperature interval of ≈500-550ºC in accordance with the mineral assemblage. Taxaquara and Ribeira Shear Zones present similar tectonic setting and deformation pattern, stress flow (25-35 MPa to SGR samples) and strain rate (10^{-12} $s^{-}1$) suggesting that the southern part of Ribeira belt was deformed under mid-crust conditions with quartz viscosity of ≈10^{18}-10^{19} Pas.

RESUMO

A Zona de Cisalhamento de Taxaquara (TSZ), NE-SW e dextral, corresponde a uma grande estrutura do tipo transcorrente pertencente à Faixa Ribeira (SE Brasil) desenvolvida durante o Ediacarano – Cambriano e relacionada com a orogenia Brasiliana – Pan Africana. A TSZ foi estudada em sua porção sudoeste a partir de trabalhos de campo e análises microestruturais, orientação cristalográfica preferencial (CPO) e de vorticidade a fim de inferir as condições de deformação (temperatura), *stress flow*, *strain rate* e viscosidade do quartzo. A TSZ é caracterizada por intensa foliação milonítica verticalizada (N062E/70SE) com lineação de estiramento sub-horizontal a obliqua com caimento preferencial para NE. As rochas compreendem milonitos ortoderivados intensamente deformados com assembleia mineral que reflete deformação no facies xisto-verde alto, com matriz composta por quartzo + feldspato + biotita + muscovita ± epidoto, dentro do campo de estabilidade da biotita e do epidoto. Rotação de subgrão (SGR) compreende o principal mecanismo de recristalização do quartzo com pequena contribuição de migração de borda de grão (GBM). Porfiroclastos de feldspato demonstram deformação rúptil (microfalhas, fraturas) e dúctil formando mantos de recristalização bem desenvolvidos em volta dos porfiroclastos. As amostras analisadas compreendem uma esteira faixa em relação ao número de vorticidade a partir do método de porfiroclastos rígidos (W^{RP}_m ≈ 0.43-0.70) o que sugere que o cisalhamento se deu em condições de strain moderado a alto. Resultados a partir do método δ/β, por sua vez, demonstra variação entre cisalhamento puro ($W^{\delta/\beta}_m$ ≈ 0.24-0.47) e simples ($W^{\delta/\beta}_m$ ≈ 0.85-0.99) ao longo do strike da TSZ. Essa variação também é demonstrada a partir da variação de geometria do CPO entre simetrias monoclínicas a ortorrômbicas. Os dados sugerem concordância com as inferências regional de que a TSZ se desenvolveu em um sistema transpressivo, porém com predomínio do cisalhamento simples sobre o puro na área estudada. Análises de CPO de quartzo sugerem contribuição dos sistemas de deslizamento 'basal-<a>' e 'rhomb-<a>' para amostras do setor NE da TSZ, sendo que os sistemas 'rhomb-<a>' e 'prism-<a>' predominam em amostras localizadas a 3 km SW da região NE. Os dados combinados sugerem 500-550°C como intervalo para temperatura de deformação concordante com assembleia mineralógica da matriz. As Zonas de Cisalhamento de Taxaquara e Ribeira apresentam contexto tectônico, *stress flow* (25-35 MPa para amostra com SGR) e *strain rate* (10^{-12} s^{-1}) semelhantes sugerindo que a região sul da Faixa Ribeira foi deformada em condições de crosta continental média com viscosidade do quartzo em torno de ≈10^{18}-10^{19} Pas.

SUMMARY

1. INTRODUCTION

The late evolution of the Neoproterozoic Ribeira belt (RB) in SE Brazil is dominated by a Late Ediacaran to Cambrian strike-slip shear zone system (Fig. 1). This system is dominated by brittle-ductile to ductile deformation and characterized by an anastomosing net of mainly dextral strike-slip shear zones with a minimum extension of about 1,000 km and individual displacements ranging from few to hundreds of kilometers (Campanha, 2002; Campanha and Brito Neves, 2004). Ebert and Hasui (1992) and Ebert et al. (1996) suggested a transpressive regime through strain partitioning between coeval and subparallel folds, ductile thrusts and strike-slip shear zones accommodating large orogen-parallel movements and shortening. This tectonic regime is also proposed by Machado and Endo (1993), Hackspacher and Godoy (1998), Dantas et al. (2000) and Egydio-Silva et al. (2002) and quantified through strain analysis indicating that the strike-slip deformation was not only due to plane strain simple shear, but also included a contractional pure shear component suggesting a transpressional regime (Fiori, 1985; Ebert et al. 1996; Campanha and Sadowski, 2002; Faleiros et al., 2016).

The Taxaquara Shear Zone (TSZ) is one of the first transcurrent structures of regional importance identified within the RB (Hennies et al., 1967; Campanha, 2002). Great importance was attributed to its role in tectonic compartmentation because it separates different terranes to the north and south (Hasui, 1973, 1975; Hasui and Sadowski, 1976; Campos Neto, 2000; Campanha, 2002). However, it has not been extensively studied since its original recognition. This work aims to fill this lack of information investigating the TSZ through based-field observations and advanced techniques like quartz crystallographic preferred orientation (CPO), grain statistics, microstructural and vorticity analysis in samples distributed towards the strike of the shear zone. These results will provide information about its tectonic regime (i.e. transpressional or transtensional) and deformation conditions (mainly temperature and mechanisms of recrystallization).

The results suggest the Taxaquara Shear Zone was affected by a transpressional regime. Quartz and feldspar microstructures and mineral assemblage indicate mylonitization process under upper greenschist metamorphic facies within biotite metamorphic zone with deformation temperature yielding 500-550°C. Opening-angle thermometer based on quartz CPO analysis also support its deformation temperature interval. Quartz grain statistics, supported by microstructural data, shows that subgrain rotation (SGR), with minor contribution of grain boundary migration (GBM) is the main mechanisms of dynamic recrystallization for quartz to all samples towards the strike of TSZ.

2. GEOLOGICAL SETTING

2.1. Ribeira belt

The Ribeira belt (RB) is a NE-trending accretionary-to-collisional orogen related to the assembly of West Gondwana during the Neoproterozoic (Almeida et al., 1973; Hasui et al., 1975; Campanha and Sadowski, 1999; Campos Neto, 2000; Heilbron et al., 2004; G. A.C. Campanha et al., 2016). It is composed by a set of tectonostratigraphic terranes with ages ranging from Paleoproterozoic to Neoproterozoic and with a voluminous arc-related, tardi- and post-collision granite magmatism (≈630 - 580 Ma). During the late Ediacaran to Cambrian (≈600 - 510 Ma) it underwent a subsequent orogen-parallel, crustal-scale transcurrent shearing system related to an oblique collision between the Paranapanema, São Francisco, Luís Alves and Congo cratons, giving rise to the Brazilian Southeastern Shear Zone System (e.g., Campanha, 2002; Campanha and Brito Never, 2004; Faleiros et al., 2010, 2011; Campanha et al., 2016).

This shear zone system is dominated by brittle-ductile to ductile transcurrent character with a preferential dextral movement (Campanha and Sadowski, 1999; Campanha, 2002). Ebert and Hasui (1992) and Ebert et al. (1996) indicate a transpressive regime through strain partitioning between coeval, subparallel folds, ductile thrusts and strike-slip shear zones accommodating large orogen-parallel movements and shortening. This tectonic regime is also described by Machado and Endo (1993), Hackspacher and Godoy (1998), Dantas et al. (2000) and Egydio-Silva et al. (2002) and quantified through strain analysis indicating that the strike-slip deformation was not only due to plane strain simple shear, but also included a contractional pure shear component suggesting a transpressional regime (Fiori, 1985; Ebert et al. 1996; Campanha and Sadowski, 2002; Faleiros et al., 2016).

The Taxaquara Shear Zone (TSZ) was originally recognized in a segment of ca. 150 km covered at its tips by the Paleozoic Paraná basin at west and the Cenozoic São Paulo basin at east (Fig. 1). In this sector, the TSZ separates the São Roque Group to north from the Votuverava Group and Embu Complex to the south as well it cuts several Ediacaran tardi- and post-tectonic granites (Janasi et al., 2001; Leite et al., 2007). Its continuity to the east of the São Paulo basin is generally considered as the Guararema Shear Zone (e.g., Hasui, 1973, 1975; Hasui and Sadowski, 1976; Campos Neto, 2000). The TSZ displays a NE-SW structural trend parallel to the main orientation of Ribeira belt and places side by side units with distinct structural style, metamorphic grade and geochronological evolution.

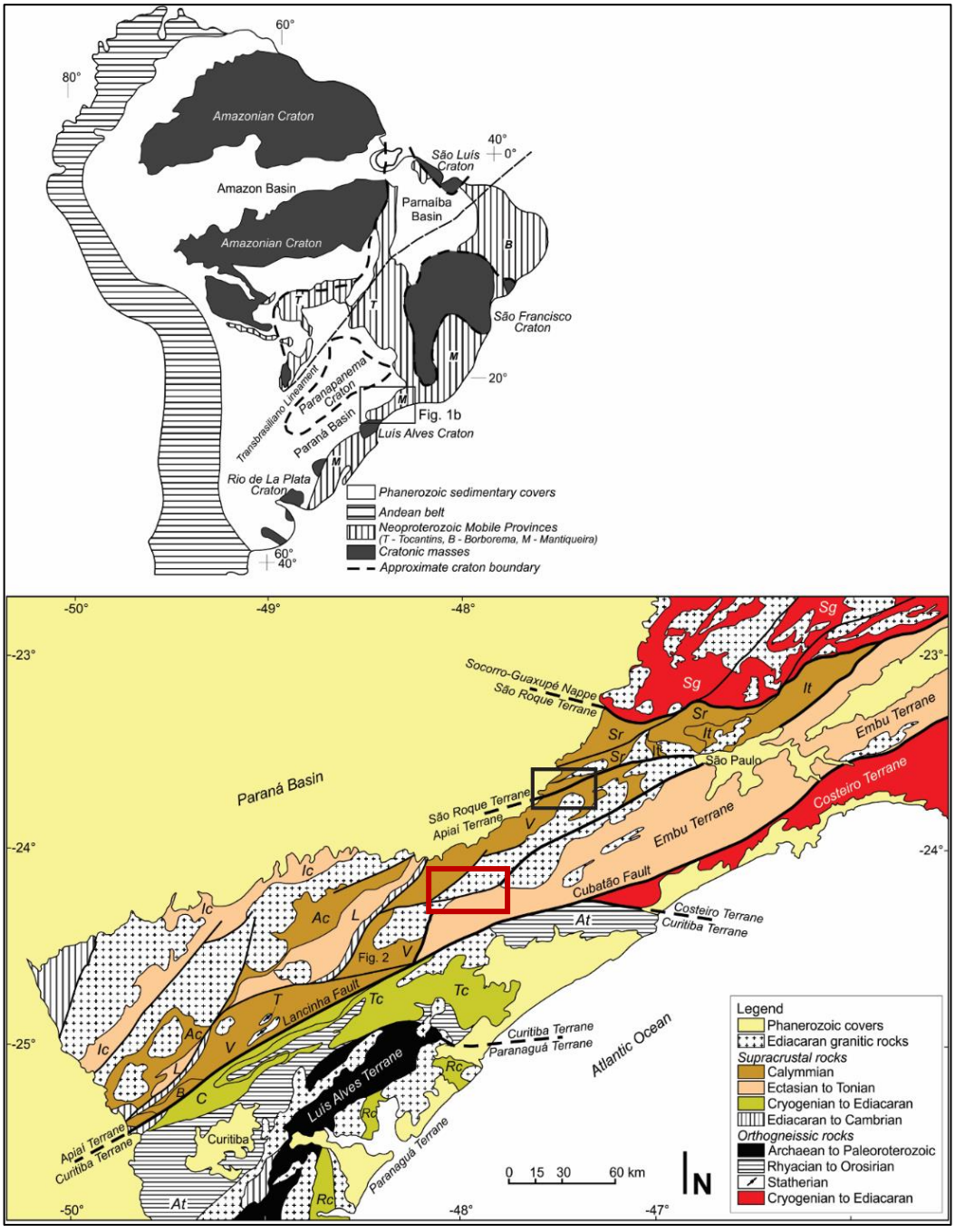

Figure 1. Simplified geotectonic map of part of South America and of the southern portion of the Ribeira Belt. Geological units: Itaiacoca Group (Ic), Água Clara Formation (Ac), Lajeado Group (L), Votuverava Group (V), São Roque Group (Sr), Serra do Itaberaba Group (It), Tigre Gneiss (T), Capirú Formation (C), Turvo-Cajati Formation (Tc), Rio das Cobras Formation (Rc), Atuba Complex (At) (Campanha et al., 2015). The black rectangle delimits the study area and the red rectangle correspond to study area of Ribeira Shear Zone in Faleiros et al. (2010).

2.2. Study area

The studied area is located at the TSZ westernmost outcropping region between the Pilar do Sul town and Bairro dos Leites district (Fig. 2). It separates a wedge of São Roque Group metasediments to the north, from the metavolcanic-sedimentary rocks of the Votuverava Group plus the Pilar do Sul and Piedade granite suites to the south.

The São Roque Group, located in the northern region, is composed of metamorphic low-grade metasedimentary rocks and displays a dominant NE-SW structural trend. Detrital zircons show an important Riacian contribution (ca. 2200 Ma, U-Pb LA-ICP-MS; Henrique-Pinto et al., 2015; Campanha et al., 2016) and with younger grains at ca. 2000 Ma. The southern region is mainly composed of the Votuverava group, which is intruded by the Pilar do Sul (ca. 600 Ma, U-Pb TIMS monazite; Leite et al., 2007) and Piedade (ca. 605 Ma, U-Pb TIMS zircon; Janasi et al., 2001) igneous suites (Fig. 2). In contrast with the São Roque Group, the Votuverava Group is composed of distal turbidites with significant basic magmatism represented by concordant lenses of metamorphosed mafic rocks (Campanha et al., 2016, 2017).

It displays a main NNW-SSE structural trend orthogonal to the TSZ and shows an east to west transition from low-grade to medium-grade metamorphism. Detrital zircon data show Orosirian-Riacian contribution (ca. 1800-2200 Ma, U-Pb LA-ICP-MS; (Campanha et al., 2016) with minor Archean ages (ca. 2800-3200 Ma, U-Pb LA-ICP-MS; Campanha et al., 2016) and minimum age at ca. 1400 Ma. The metabasites of the Votuverava group with an ca. 1300 Ma crystallization age (U-Pb SHRIMP zircon; Campanha et al., 2016) and show a Neoproterozoic metamorphic overprint (ca. 600-700 Ma, U-Pb SHRIMP; Campanha et al, 2016).

In the study area, the TSZ is represented by an anastomosed mylonitic zone with a thickness varying between hundreds of meters to two kilometers (Fig. 2). The shear zone mainly affected the ≈600 Ma igneous rocks of the Pilar do Sul and Piedade suites giving rise to quartz-feldspar mylonites with feldspar porphyroclasts. The shear zone is a steeply inclined planar structure, striking NE-SW with a parallel mean foliation trending 062/70SE (strike/dip), which is also the axial plane of tight folds (Fig. 3E). It has a sub-horizontal to oblique stretching lineation, mainly marked by stretched quartz with an orientation distributed along a 90-degree section of a girdle parallel to the main foliation, with maximum concentrations towards the NE (Fig. 4A). The TSZ accommodates an oblique displacement and its dextral shear sense is indicated by mesoscopic structures such as S/C structures, asymmetric porphyroclasts (type-σ and type-δ) that are also internally fractured feldspar (Fig. 3B) with a smaller normal movement component (hanging wall to SE) (Fig. 4B). Structures such as S/C (Fig. 3D) are a common form of strain partitioning and, thus, partition of deformation concentrating a large portion of the simple shear component in transpressional shear zones (Tikoff and Greene, 1997).

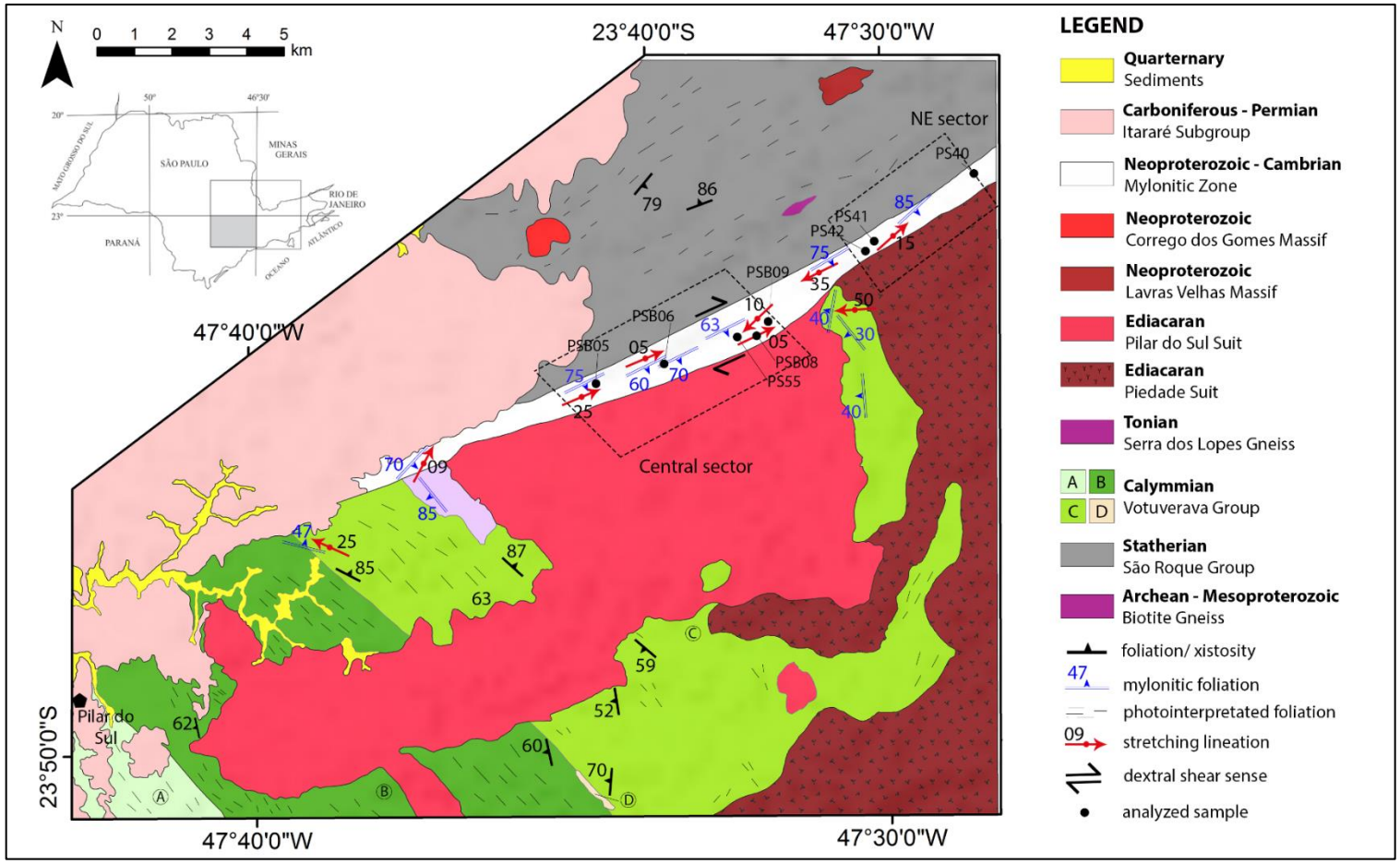

Figure 2. Geological map of the study area with focus on Taxaquara Shear Zone (compiled and modified from Stein et al., 1983 and Pires et al., 1989). The Votuverava Group is composed of A) sericitic and quartz phyllites; B) quartz-muscovite and muscovite schists; C) mica-quartz and micaschists; D) paragneiss.

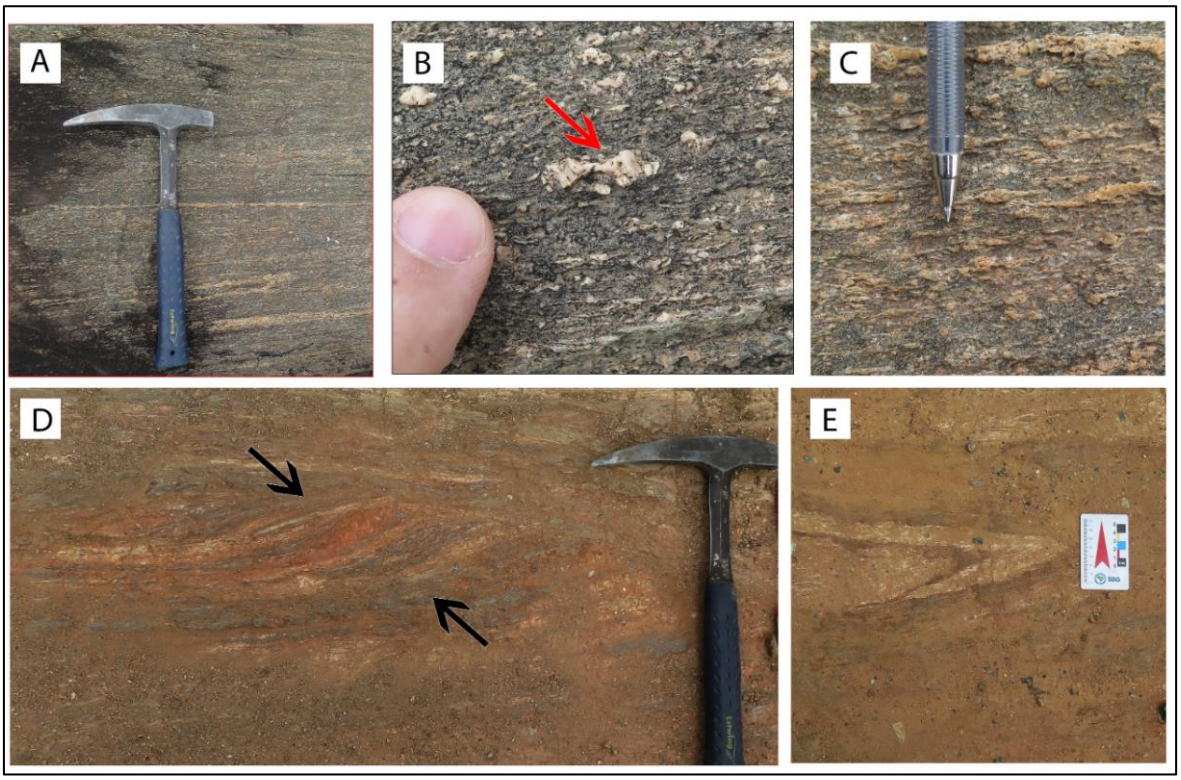

Figure 3. Field structures related with Taxaquara Shear Zone. A) layered mylonitic granite; B) antithetical microfaulting (normal movement) in feldspar porphyroclast; C) streaks of stretched feldspar parallel to stretching lineation; D) S/C fabric with dextral shear sense (black arrows indicate σ_1 position); E) tight fold with axial plane parallel to mylonitic foliation.

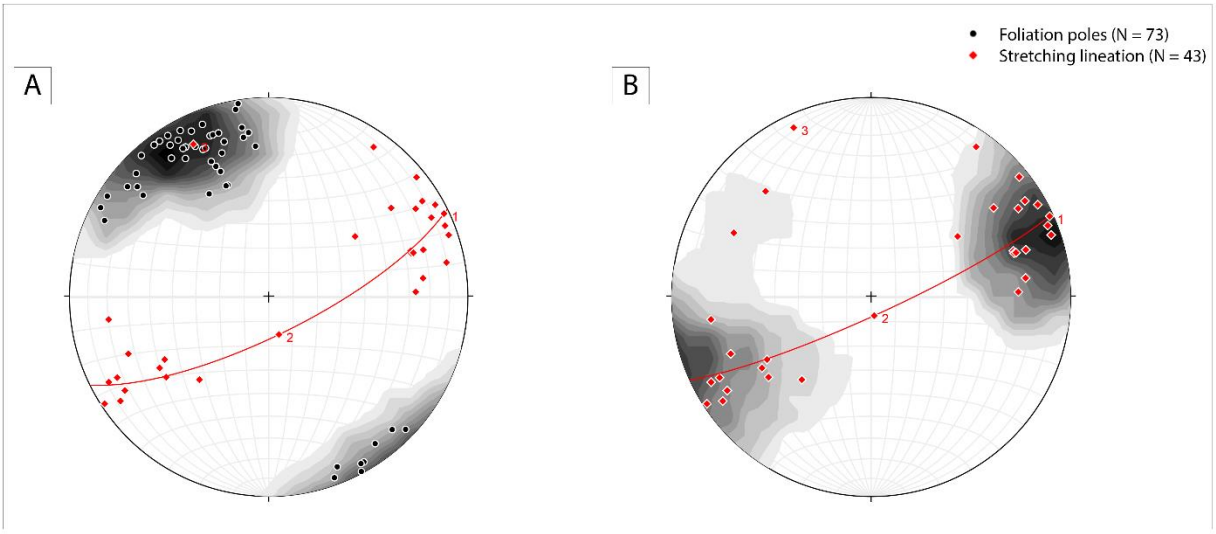

Figure 4. A) Stereogram (lower hemisphere, equal area projections) with mylonitic foliation (mean vector 062/70SE; strike/dip) and stretching lineation along the shear plane; B) statistical contour of stretching lineation.

3. MICROSTRUCTURAL ANALYSIS

The petrographic studies were carried out at the Petrography Microscope Laboratory (University of São Paulo) and at Petrography Laboratory of School Earth, Atmosphere and Environmental of Monash Univeristy.

Thirteen thin sections of mylonites samples from the northeastern and central sectors of TSZ (Fig. 2) cut perpendicular to foliation and parallel to stretching lineation (*XZ section*), were analyzed to characterize mineral assemblages and microstructures to estimate the kinematics and deformation conditions. Results are summarized in tables 1 and 2, respectively.

To support microstructural analysis, fabric domains (quartz ribbons) of eight samples were chosen and classified through a number of quantitative measures. Quartz fabric domains were manually digitized using ArcGIS (*version 10.0)* with 250-300 grains per domain to ensure a sound statistical representation. These domains were analyzed using *PolyLX* (http://petrol.natur.cuni.cz/~ondro/polylx:home) toolbox in MATLAB to quantify the following statistical parameters: (i) area; (ii) grain roundness; (iii) grain long axis orientation; (iv) axial ratio; (v) Feret diameter; (vi) grain lobateness (PARIS factor; Heilbronner and Tullis, 2002). Results are summarized in table 3.

3.1. Mineralogy and microstructures

The protolith to the mylonites analyzed samples are mainly the Pilar do Sul and Piedade granitic suites cross-cutted by TSZ. Leite et al. (2007) detailed the Pilar do Sul as a foliated medium- to coarse-grained inequigranular muscovite-biotite monzogranite in its border and fine-grained muscovite-biotite granite within the suit core. They also detailed the Piedade suit and characterized as porphyritic muscovite-biotite granodiorite to monzogranite with a foliation of moderate intensity defined by the alignment of tabular pink alkali feldspar megacrysts of 1-2 cm and of porphyritic biotite monzogranite with 1-2 cm pink alkali-feldspar megacrysts. These suits were also detailed by Janasi et al. (2001), Leite (1997), Leite et al. (2006) and Martins (2001).

TSZ mylonites generally have well-developed lineations defined by elongate quartz, streaks of recrystallized feldspar (Fig. xx) and mica (biotite and muscovite) and sub-vertical mylonitic foliations forming LS tectonites and ultramylonites. The samples analyzed are derived from these granitoids rocks and its matrix consist dominantly of quartz + feldspar + biotite + muscovite ± hornblende ± epidote ± chlorite. Plagioclase and alkaline feldspar occurs as porphyroclasts (0.1-1.0 cm in thin section) and tourmaline, garnet, apatite, titanite and opaque occurs as accessories, and can be classified as igneous relicts in microstructural equilibrium because it is not observed any metamorphic reactions that would led to the formation of these minerals (table 1). Chlorite may occur replacing biotite. The samples present

20–60% of matrix and the remainder is porphyroclasts, and vary from protomylonites to mylonites according to the classification of mylonites in Trouw and Passchier (2010).

The samples are similar and quartz, feldspar, biotite and muscovite are recrystallized forming the mylonitic matrix with texture varying from lepidoblastic to granoblastic as end members. Anastomosed quartz ribbons are common and are stretched parallel wrapping around the alkaline feldspar and plagioclase porphyroclasts showing the plastic condition of deformation process. The matrix assemblage quartz + feldspar + biotite + muscovite + epidote indicates a low-grade metamorphism (greenschist facies) within biotite zone with its intense syn-kinematics recrystallization.

Janasi et al. (2001) and Leite et al. (2007) mention the presence of hydrothermal alteration mainly in Pilar do Sul suit with pneumatolithic-hydrothermal stages with endogreisens, meter-sized, elongated bodies commonly showing zoning from granite to muscovite greisen, quartz greisen and a central body of quartz vein. Megacrysts of feldspar being replaced by sericite taking advantage of the twinning planes (Fig. 8A) is a common feature suggesting sericite alteration at low temperature due interaction with magmatic fluids.

3.2. Kinematic indicators

The main kinematic indicators are asymmetric porphyroclasts, mica fish and quartz shape preferred orientation oblique to main shear plane. Alkaline feldspar and plagioclase comprise 80% of porphyroclasts and are generally rotated forming mostly σ clasts (Figs. 5 B, C, D, E), and less commonly δ clast. Porphyroclasts type-ϕ are rare. The asymmetry can be identified by streaks of mica and quartz ribbons which wrap around the porphyroclasts, and quartz and feldspar are recrystallized forming asymmetric porphyroclast tails (Figs. 5 C, D, E).

Coarse muscovite form fish geometries in a few samples (samples PS – 40 A, PS-40 B in Fig. 5 A, B and Table 2). Biotite fish is less common because of more intense recrystallization. Quartz grains oriented obliquely to foliation is common, observed in 90% of the samples (Fig. 5 F). Mostly kinematic indicators described display a dextral movement which is congruent with field observations.

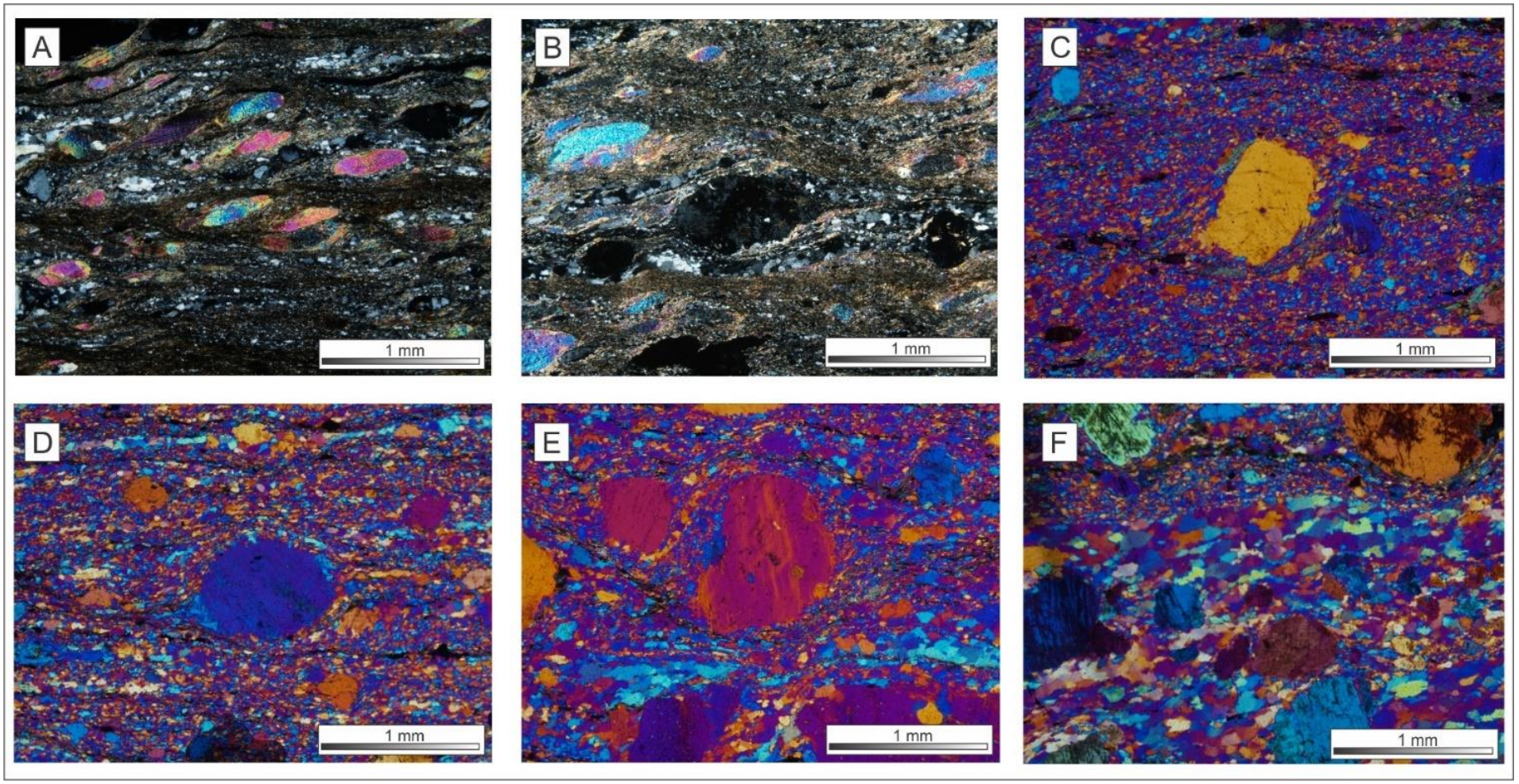

Figure 5. Photomicrographs of TSZ mylonites illustrating main kinematic indicators (XZ section; A-B: cross-polarized light; C-D: cross-polarized light with gypsum plate). A) muscovite fish; B) muscovite fish and porphyroclast type-σ; C, D, E) feldspar porphyroclasts type-σ wrapped by quartz; F) quartz oblique shape foliation. All kinematic indicators mark a dextral movement.

3.3. Quartz grain statistics

The samples present similar grains statistics results in all analyzed parameters. The quartz grain mean area corresponds to ≈2900µm² with ≈2480 µm² standard deviation indicating a heterogeneous population from small to large grains. It is also observed regards Feret diameter varying from ≈11 µm to ≈181 µm with average Feret diameter of ≈53 µm. In all cases, they present prismatic shape (≈1.60 mean axial ratio) and oblique major axis in relation to the horizontal shear plane (≈11º mean orientation) (fig. 6A), reinforcing the dextral shear sense.

The relation between Feret diameter and grain lobateness (PARIS factor; Heilbronner and Tullis, 2002) results in a cluster (Fig. 6B) suggesting similarities in diameter (≈42µm to ≈66µm) and lobateness (≈3.5% to ≈6.40%). This observation is also clear in the logarithmic plot of Feret diameter (D) multiplied by lobateness (L) proposed by Hunter (2017) which indicates a flat pattern (Fig. 6C B). Once it's known that grain diameter is strictly linked with the dominant recrystallization mechanisms (Stipp et al., 2010), these results suggest that all the samples along the strike of the shear zone, from central to NE sector, are composed by quartz grains affected by similar recrystallization mechanisms and, therefore, same deformation temperature.

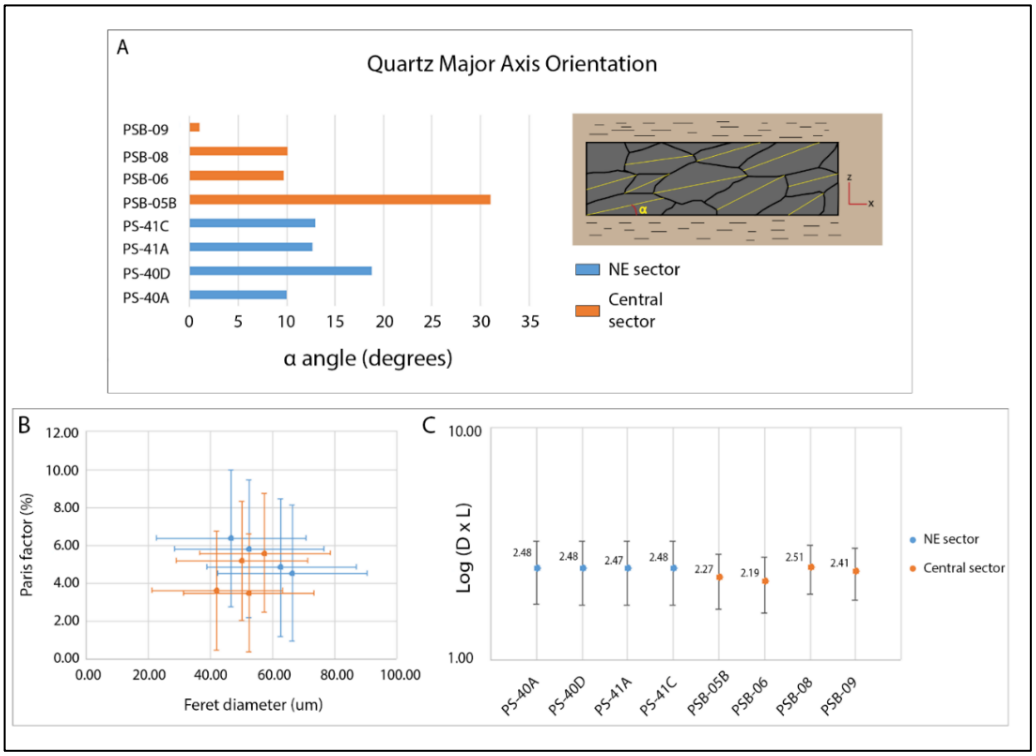

Figure 6. Quartz grain statistics based on digitized grains in ArcGIS (version 10.0) and analyzed using PolyLX toolbox in MATLAB. A) Quartz major axis orientation in relation with horizontal shear plane measured in XZ section indicating the obliquity present in all samples; B) grain lobateness (PARIS FACTOR; Heilbronner and Tullis, 2002) plotted against grain size (Feret diameter) for samples from NE and Central sectors with a strong cluster result considering error bars (standard deviation values); Logarithmic plot of lobateness multiplied by diameter (L x D; Hunter, 2017) for samples from NE and Central sectors with a flat result suggesting no variation between samples along strike of TSZ.

4. QUARTZ AND FELDSPAR DEFORMATION CONDITIONS

4.1. Quartz recrystallization mechanisms

Quartz phase occurs within the recrystallized mylonitic matrix as very fine grains (< 0.01 mm) and in anastomosed ribbons parallel to the stretching lineation and commonly wrapping around porphyroclasts suggesting the ductile deformation condition.

Quartz presents interlobate grain boundaries, sometimes poorly defined, rarely polygonal, prismatic shape (1.60 mean axial ratio), inequigranular grains with diameter varying from ≈11 µm to ≈181 µm with average Feret diameter of ≈53 µm, ondulose extinction and deformational bands (Fig. 7). These features suggest mechanisms of dynamic recrystallization where both subgrain rotation (SGR) and grain boundary migration (GBM) plays a role (Stipp et al., 2002a, 2002b; Passchier and Trouw, 2005). Although not frequent, polygonal grains boundaries are observed (Fig. 7 B, C) indicating small contribution of static recrystallization. Bulging (BLG) are observed and can be related with shear zone exhumation with decrease in temperature (Fig. 7 B, C). The grain statistics regards Feret diameter is in good agreement with dominance of SGR and minor GBM contribution according to grain size limits between BLG, SGR and GBM in Stipp et al. (2002b).

Stipp et al. (2002a) and Faleiros et al. (2010, 2016) correlate the dominant deformational mechanisms operating during recrystallization to temperature in nature where bulging (BLG) is dominant between 280-400°C and SGR in 420-550ºC interval where GBM predominates above ≈550°C. Once these relationships are established, the quartz microstructures suggest deformation temperature which spans the interval from ≈420 to ≈550°C due important contribution of SGR and GBM recrystallization mechanisms (table 2) which in congruent with greenschist metamorphic facies.

4.2. Feldspar recrystallization mechanisms

Feldspar is an abundant phase in TSZ mylonites. It occurs within recrystallized matrix (< 0.01 mm) and as porphyroclasts (0.1 to 1.0 cm) and its deformations plays a role in development of mylonitic fabrics. Although feldspar deformation temperatures are not consensus in literature, Borges and White (1980), Simpson (1998) and Tullis (2002) propose that BLG becomes an important dynamic recrystallization mechanisms between 400° and 600°. Dislocation climb and recovery processes initiates at lower temperature (around 450°C) and SGR plays an important role in temperatures above 500-550°C (Simpson, 1985; Gapais, 1989; Pryer, 1993).

The feldspar porphyroclasts present evidences of fractures and internal microfracturing frequently observed in all samples (Fig. 8A). These microstructures suggest a low deformation temperature (< 300°C; Passchier and Trouw, 2005) where feldspar is deformed under brittle

conditions. Trails of fine feldspar grains (< 0.1 mm) filling these internal microfractures and fine coursed mantle of recrystallization surrounding porphyroclasts without transitional size grain zone suggest an important dynamic recrystallization (BLG) at medium grade conditions (Fig. 8F). Twinning deformation and ondulose extinction suggest contribution of dynamic recrystallization via SGR (Fig. 8C). Myrmekites and flame pertites induced by deformation occur along the edge of porphyroclasts in minor proportion (Fig. 8B, D).

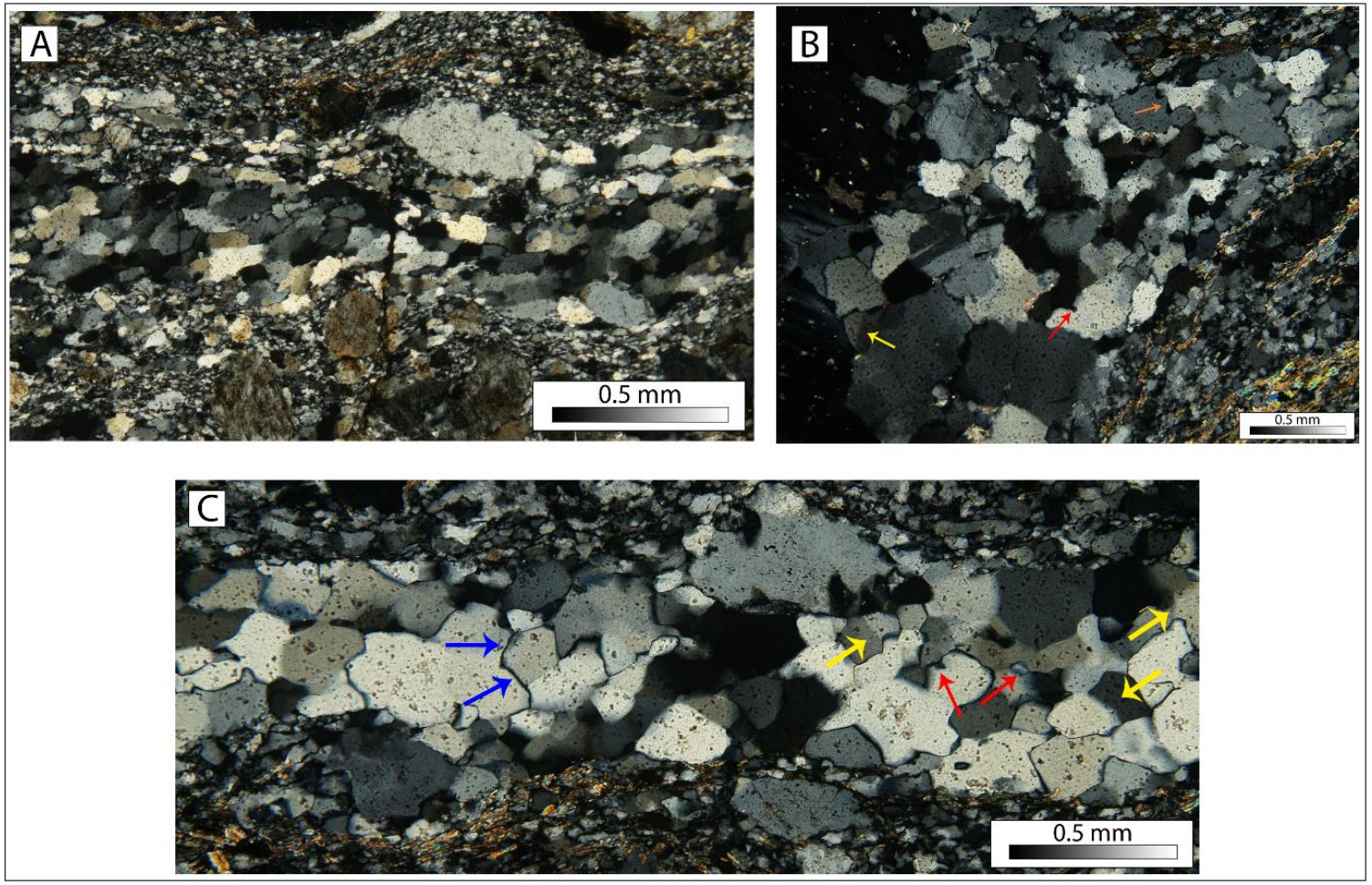

Figure 7. Photomicrographs of TSZ mylonites regarding quartz microstructures (cross-polarized light, XZ section). A) Quartz SGR with oblique grain shape fabric with dextral shear sense; B) Quartz ribbons with BLG (red arrow), SGR (yellow arrow), and GBM (orange arrow) evidence; C) Quartz ribbons parallel to foliation with abundant SGR evidence (yellow arrow), BLG in minor proportion (red arrow) and polygonal boundaries (blue arrows) suggesting contribution of static recrystallization.

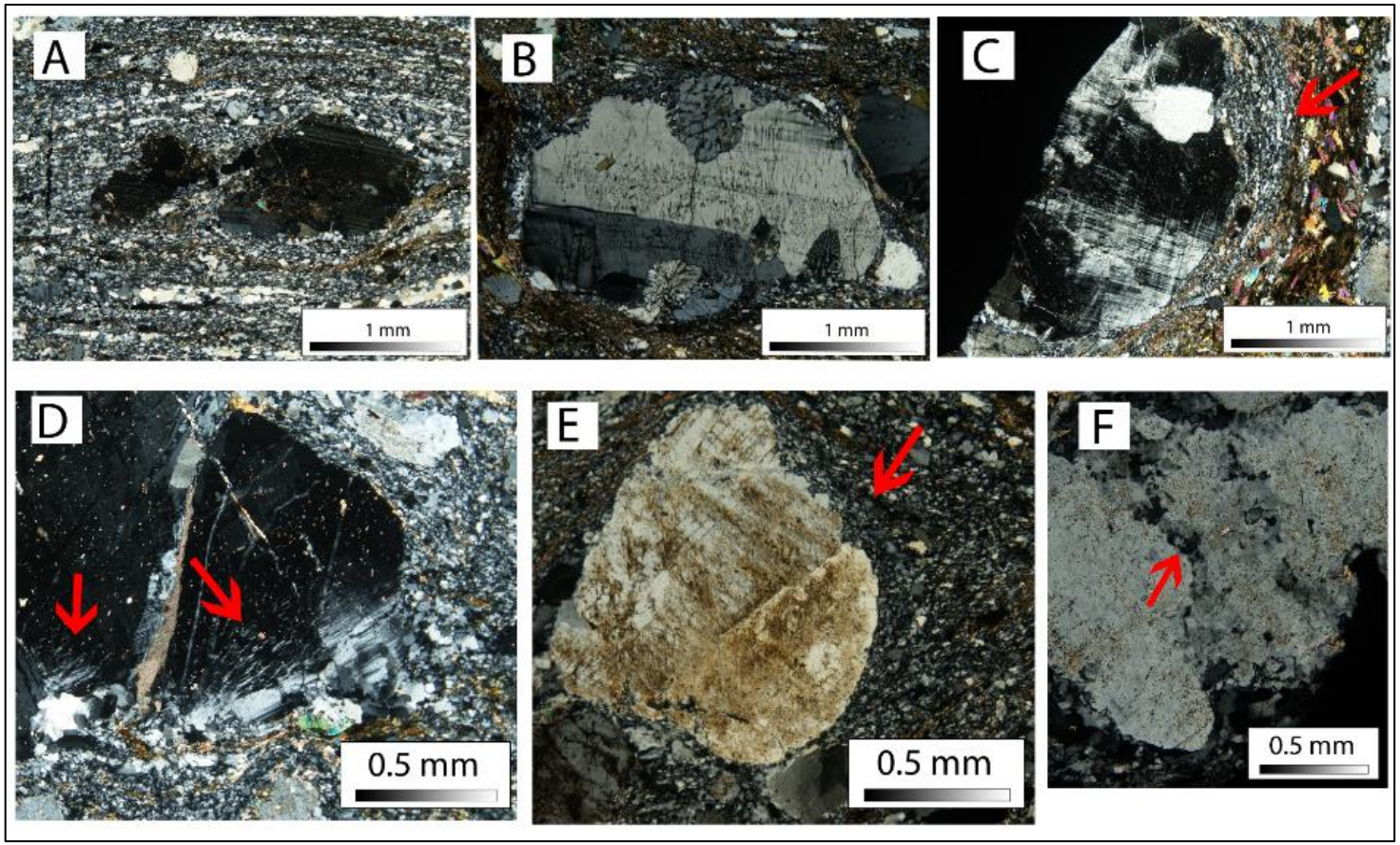

Figure 8. Photomicrographs of TSZ mylonites regards feldspar deformation (cross-polarized light, XZ section), red arrows indicate microstructures. A) antithetical normal microfraulting within recrystallized feldspar-bearing matrix (sample PS-55); B) myrmekite induced by deformation along margins of feldspar porphyroclasts (PS-41B); C) mantle of recrystallization (feldspar ± quartz ± sericite) surrounding a feldspar porphyroclasts with ondulose extintion and subgrains suggesting SGR mechanism of recrystallization (PS-42B); D) Flame pertites induced by deformation in K-feldspar porphyroclast (PS-42B); E) feldspar porphyroclast with sericite alteration surrounded by mantle of recrystallization (PS-41A); F) tracks of fine-grain feldspar suggesting BLG mechanism of recrystallization individualizing subgrains (PS-42B).

5. QUARTZ CRYSTALLOGRAPHIC PREFERRED ORIENTATION

Crystallographic preferred orientation (CPO) is observed in many quartz-bearing rocks as the result of tectonic processes (Skrotzki, 1994) and develop due to intracrystalline slip where dislocation movement occurs preferentially along lattice planes oriented at low angles to the critically resolved shear stress (Schmid factor; Schmid and Boas, 1935). Quartz CPO is commonly investigated by focusing on the orientation of its [c] axis. The preferential slip plane defining slip direction is referred to as the slip system and is strictly related with quartz deformation (Lister, 1977; Schmid and Casey, 1986; Keller and Stipp, 2011). At lower temperatures and strain, slip commonly occurs along the 'basal-<a>' system followed at higher temperature by 'rhombohedral-<a>' slip and at temperatures above 500°C slip along 'prismatic-<a>' and grain boundary migration (GBM) are observed (Stipp et al., 2002a).

Links between deformation conditions and CPO patterns are observed. A relation with finite strain and the degree of [c] axis preferred orientation has been found in modelling (Etchecopar, 1977; Lister and Hobbs, 1980), deformation experiments (Tullis and Yund, 1977; Dell'Angelo and Tullis, 1986; Dell'angelo and Tullis, 1989; Heilbronner and Tullis, 2006) and natural deformations (Schmid and Casey, 1986; Stipp et al., 2002b; Toy et al., 2008). The relationship between CPO pattern and temperature (Kruhl, 1996; Law, 2014) via opening-angle thermometer and the active dynamic recrystallization mechanisms in quartz (Faleiros et al., 2010, 2016) are also observed. The many CPO patterns that result can be used to support the interpretation of strain histories including temperature, strain magnitude and strain geometry (i.e. pure shear versus simple shear) and kinematics of naturally deformed rocks. Therefore, this approach has been an important tool in microstructural studies to support the structural evolution of shear zones (Stipp et al., 2002a; Faleiros et al., 2010; Oliot et al., 2014; Oriolo et al., 2015; Rahl and Skemer, 2016).

There are several methods to obtain quartz crystallographic preferred orientation (CPO) data. The optical petrographic microscope with a universal stage (U-stage), which has been traditionally used (Fedorov, 1982), is progressively being replaced by modern techniques, such as electron backscattering diffraction (EBSD), neutron diffraction (ND) and Fabric Analyzer (FA, Wilson et al., 2007). The comparison between these methods made by Hunter et al. (2016) shows that although FA method is unable to determine vertical [c] axis for quartz, it is the most simple method with low acquisition time, low sample preparation and with good accuracy, which makes this method the most suitable technique for routine and rapid acquisition of [c] axis poles figures across large areas.

The FA (Wilson et al., 2007) is an automated, computer controlled, polarizing microscope, designed for the spatial mapping of [c] axis orientations in optically uniaxial crystals (e.g. quartz). The data processing is undertaken using the free software *Investigator* (Wilson et al.,

2007) and [c] axis orientation maps are produced based on the 'Achsenverteilungsanalyze' (AVA) technique (Sander, 1950). For a detailed description of Fabric Analyzer functionality see (Wilson et al., 2007; Peternell et al., 2010).

Quartz [c] axis measurements were carried out at School of Earth, Atmosphere and Environmental of Monash University (Melbourne, Australia) using a Fabric Analyzer (G50). Measurements were collected from quartz-rich aggregates (ribbons). In this study, the CPOs are used to determine slip-system activated during quartz deformation, deformation temperature through opening-angle (OA) thermometer (Kruhl, 1996; Law, 2014; Faleiros et al., 2016) and vorticity studies (δ/β – method; Wallis, 1992, 1995). Data were further processed using the MTEX (https://mtex-toolbox.github.io/) toolbox in MATLAB to quantify OA and the vorticity plane (*section 6 of this work)*.

5.1. Quartz [c] axis fabric

The samples can be classified in two groups based on their different CPO patterns. The first group, located in the northeastern sector of the TSZ (Fig. 2) is characterized by symmetric (Fig. 9; samples PS-40A, PS-40B, PS-41A, PS-41B, PS-42B) to slightly asymmetric CPOs implying a dextral movement (Fig. 9; samples PS-40D, PS-41A, PS-41C, PS-42B) showing maxima subparallel to or at a small angle to the Z direction. The orientations of c-axis poles suggests activity of 'basal-<a>' and 'rhomb-<a>' slip systems based on general correlations between quartz [c] axis location and slip systems (Fig. 10 A) (Schmid and Casey, 1986).

The second group, located in the central sector of the TSZ, has a more heterogeneous CPO. Samples PS-55 and PSB-05B (Fig. 9) present patterns with two maxima between X and Y directions defining an orthorhombic symmetry. The data gap in the centre of the CPO, corresponding to 'prism-<a>' is due FA limitations makes it difficult to determine whether this slip system was activated. Samples PSB-06 and PSB-08 (Fig. 9) display an asymmetric pattern in relation to Z direction, with maxima close to Z and X direction, respectively, and circling the Y direction. Sample PSB-09 (Fig. 9) comprises a symmetric to slightly asymmetric pattern, indicating a possible dextral movement, with maxima close to the Z direction. The [c] axis location indicates a contribution of 'rhomb-<a>' slip system (Schmid and Casey 1986). Hunter et al. (2016) demonstrated that CPO with two maxima circling the Y axis obtained through FA must indicates activity on 'prism-<a>' slip system when compared with results from EBSD or ND. Therefore, it is possible that samples PSB-06, PSB-08 and PSB-09 deformed via 'rhomb-<a>' and 'prism-<a>' slip system, which would result in single girdle pattern and single maximum parallel to the Y direction.

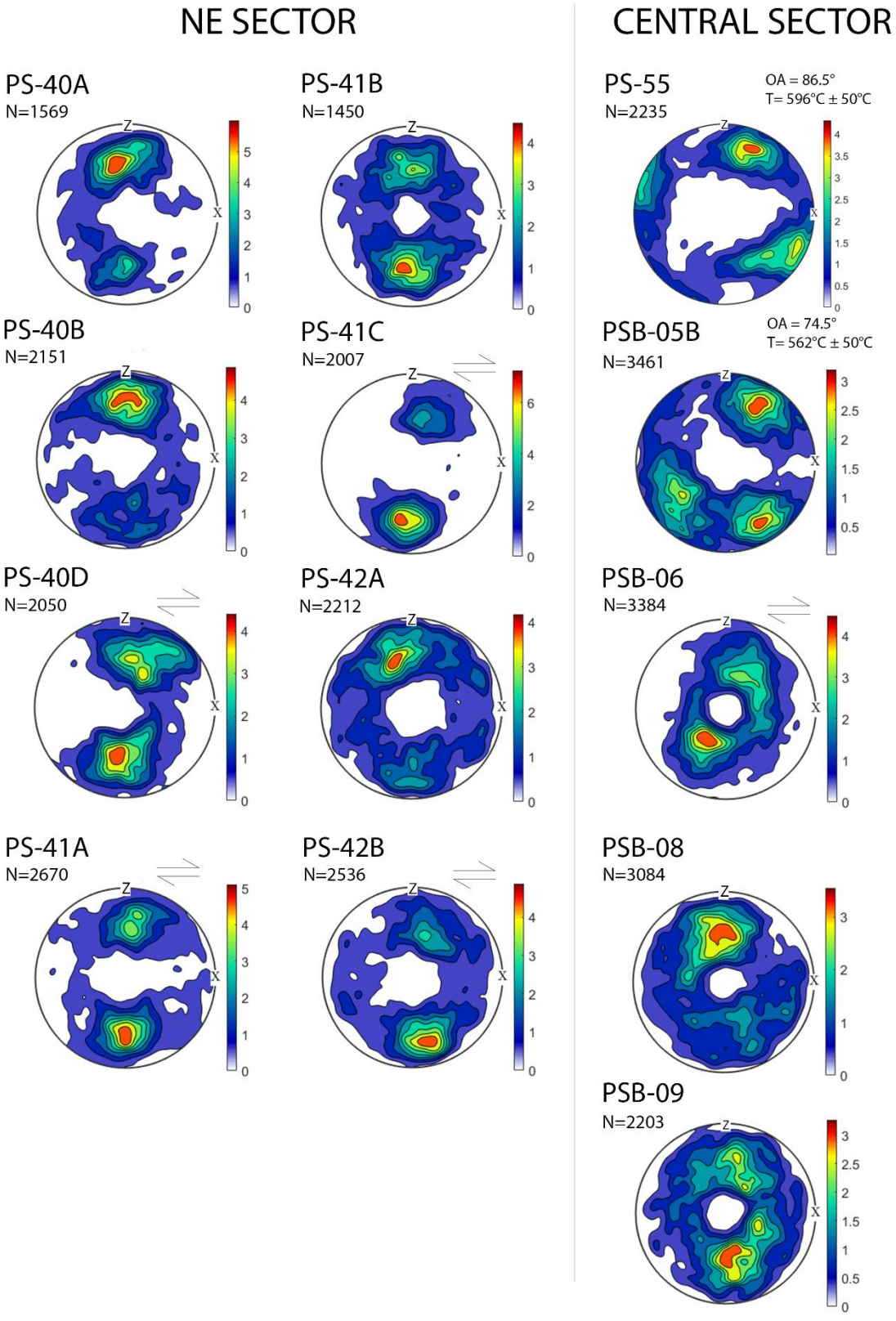

Figure 9. Quartz [c] axis fabric measured using Fabric Analyzer (FA) and processed using MTEX toolbox in MATLAB; lower hemisphere equal area projections; foliation oriented left-right and vertical, stretching lineation horizontal. Samples number and the values of [c] axis measurements are indicated upper left. Opening-angle (OA), values of temperature calculated using Faleiros et al. (2016) calibration and shear sense are indicated upper right.

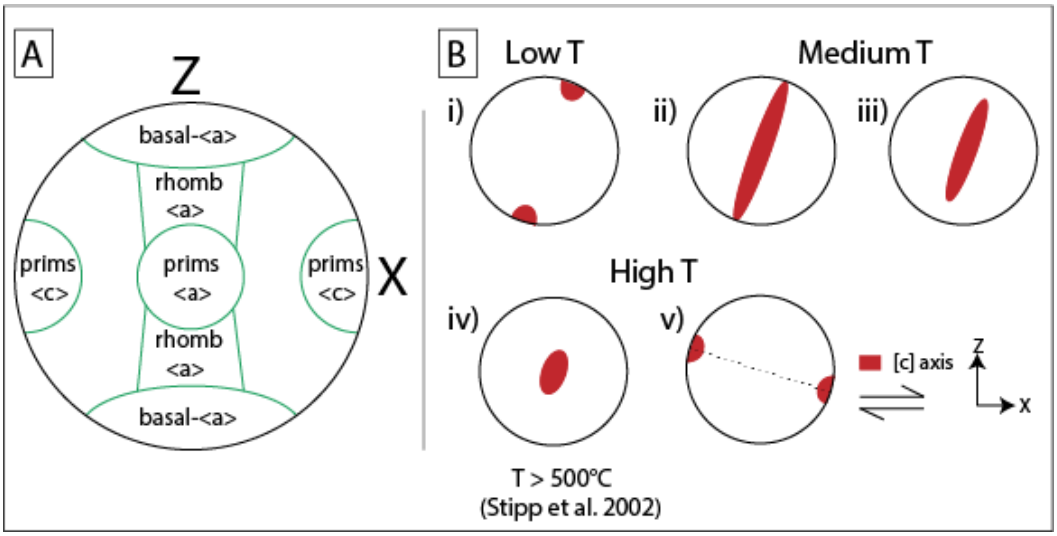

Figure 10. A) General correlations between locations of quartz [c] axes and activity of slip systems (based on Schmid and Casey, 1986). B) General quartz CPO patterns formed by simple shear under different temperatures: i) activation of 'basal-<a>' at low temperature; ii) activation of 'basal-<a>' + 'rhomb-<a>' ± 'prism-<a>' and iii) activation of 'rhomb-<a>' + 'prism-<a>' at medium temperatures; iv) activation of pure 'prism-<a>' and v) pure 'prism-[c]' at higher temperatures (modified from Passchier and Trouw, 2005).

5.1.1. Comparison between different ribbons

A comparison between different quartz ribbons and general data of quartz [c] axis from the same sample were carried out in order to determine if different structures have different [c] axis orientations which might cause mixing data disturbing the texture of [c] axis pole figure. For this, samples PSB-05B and PSB-06 were selected. Measurements were carried out using Fabric Analyzer (FA) and analysed using MTEX.

Although different numbers of measured quartz [c] axis, pole figures of general data and individual ribbons display similar geometry with orthorhombic and monoclinic symmetry for samples PSB-05B and PSB-06, respectively. Besides similar geometry, they also suggest same slip systems activities based on Schmid and Casey (1986) general correlations.

These comparisons show that different quartz ribbons have same quartz [c] axis orientation and, therefore, there is no mixing data. Besides, the same geometry and suggestion of slip systems activities are clear with 500 analysed grains. However, it is clear that when a major number of grains are measured, the pole figures tend to be well defined than the others.

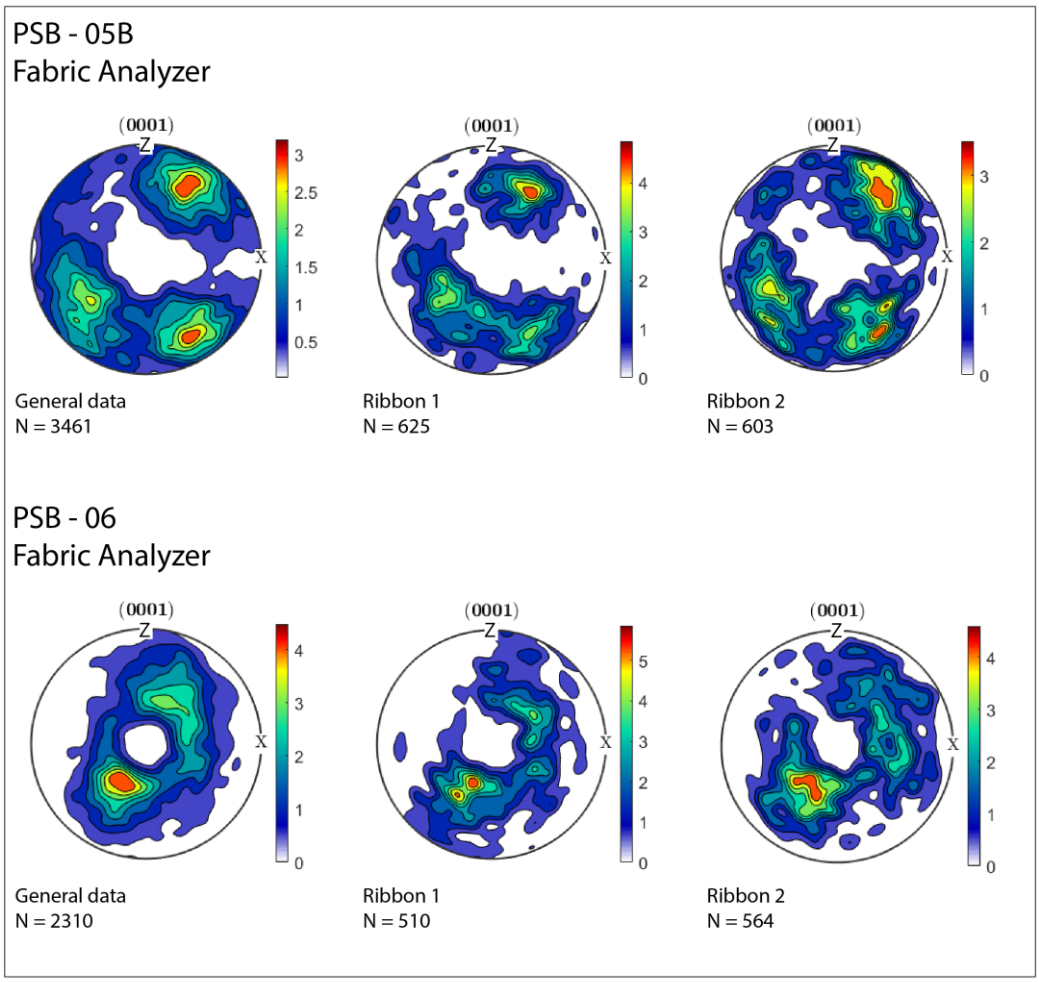

Figure 11. Quartz [c] axis fabric measured using Fabric Analyzer (FA) and processed using MTEX toolbox in MATLAB; lower hemisphere equal area projections; foliation oriented left-right and vertical, stretching lineation horizontal.

5.1.2. EBSD and FA comparison

In order to reinforce the interpretation based on Fabric Analyzer results, sample PS-41A was analysed via EBSD at LATEC-LAME laboratory (Paraná, Brazil). Measurements were made using a 20-kV acceleration voltage and 14 mm work distance. Data were analysed using MTEX toolbox in MATLAB. Although EBSD data show a pole figure more concentrated than FA, the results of quartz [c] axis from EBSD for sample PS-41A (Fig 11 A) is very similar to that from FA (Fig. 9) with symmetrical monoclinic geometry, strongly supported by pole figures of <a> and {m} axis, with maxima parallel to the Z direction from EBSD analysis (Fig. 11 A).

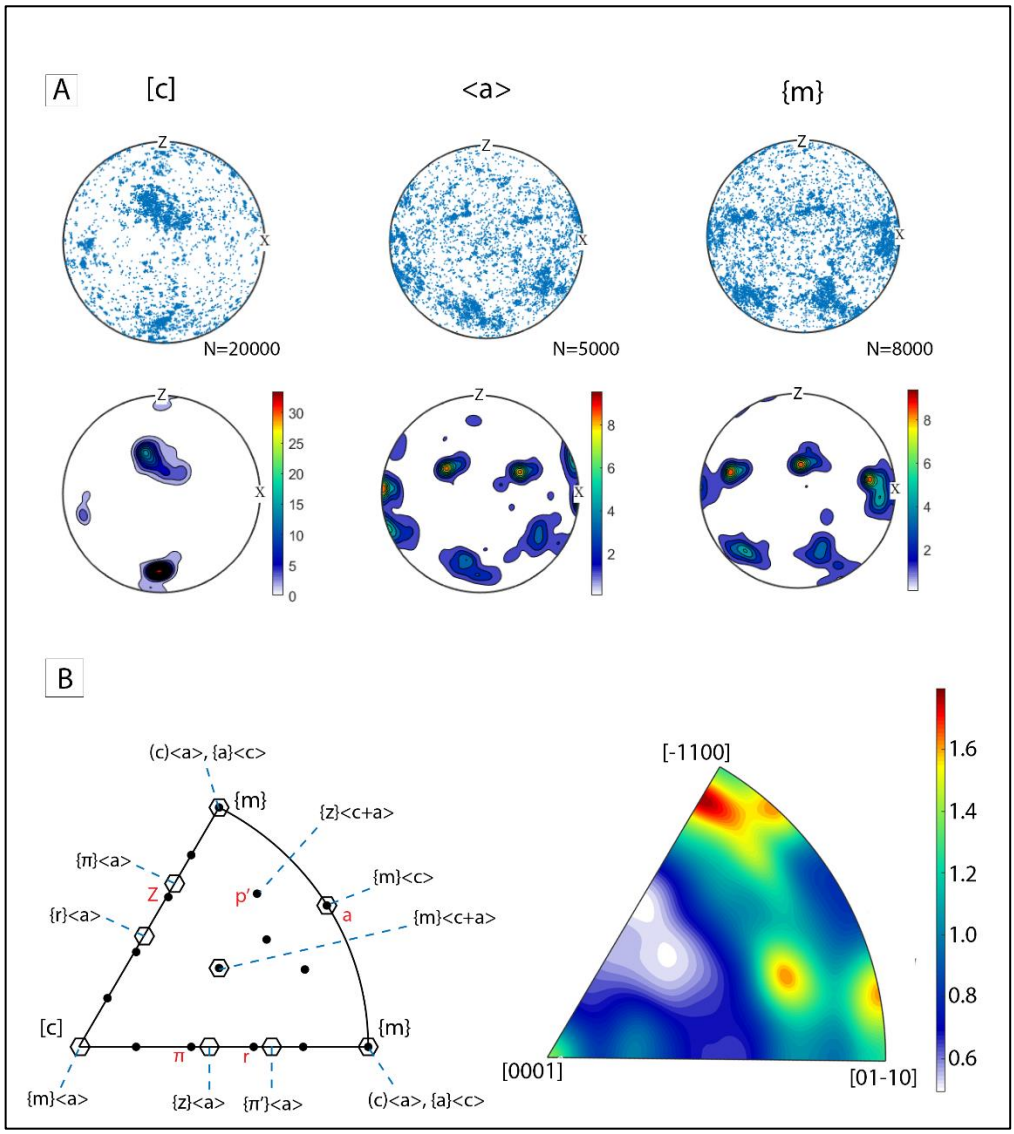

Figure 12. A) Quartz CPO measured using EBSD (Sample PS-41A); lower hemisphere equal area projections; foliation oriented left-right and vertical, stretching lineation horizontal; B) misorientation axis/angle based on correlated (i.e. nearest neighbor) data. Simplified distribution of rotation axes for common slip system is shown left (Neumann, 2000). c, a, m, r, z, π, π' correspond to crystal directions.

Regarding the slip systems, FA analysis only provide quartz [c] axis orientations which may suggest slip systems activity based on its location in pole figures (Schmid and Casey, 1986) (Fig. 10 A). Assuming that crystal slip occurred predominantly on tilt boundaries, EBSD comprises a powerful tool in crystallographic studies since it provides the orientation of all quartz axis allowing to produce misorientation angle figures to assist the interpretation of slip systems (Neumann, 2000; Wheeler et al., 2001). Based on general correlations proposed by Schmid and Casey (1986), both FA and EBSD results suggest contribution of 'basal-<a>' and 'rhomb-<a>' activities. However, misorientation angle figure based on EBSD results shows the predominance of 'basal-<a>' activity to sample PS-41A.

5.2. Opening-angle thermometer

An opening-angle correspond to the angle separating the two girdles that define a cross girdle CPO pattern (orthorhombic symmetry). Kruhl (1996) observed a positive linear correlation between OA and temperature from rocks naturally deformed and proposed it as a deformation-related thermometer. The angle increases with rising temperatures, hydrolytic weakening and with decreasing strain rates (Kruhl, 1996; Morgan and Law, 2004; Law, 2014). Since Kruhl (1996), the method has undergone minor refinements (Morgan and Law, 2004; Law, 2014) and more recently Faleiros et al. (2016) compiled and expanded the available data set of OA *versus* temperature which spans the interval from ≈250 to ≈1050°C and ≈2.5 to ≈15 kbar, being the first paper to propose a relationship to pressure.

Two samples (PSB-55, PSB-05B) display orthorhombic symmetry suggesting a type I asymmetric cross girdle (Lister, 1977) making them suitable for opening-angle thermometer analysis using Faleiros et al. (2016) equations (Eq. 1, 2). To avoid any visual bias, the OA measurements were carried out through a MTEX routine which determines the location of maxima intensities and the angle between them.

$$T(°C) = 6.9\ OA\ (degree) + 48\ (250°C\ \leq T \leq 650°C\ and\ OA \leq 87°) \quad (1)$$

$$T(°C) = 4.6\ OA\ (degrees) + 258\ (650°C \leq T \leq 1050°C\ and\ OA \geq 87°) \quad (2)$$

The OA measured by the MTEX routine are 86.5° and 74.5° for samples PS-55 and PSB-05B, respectively, which yield deformation temperatures of ≈596°C ± 50° and ≈562°C ± 50°C (Fig. 9). The temperature interval corresponds to the transition between SGR and GBM according to transition zones between dynamic recrystallization mechanisms proposed by Stipp et al. (2002) and Faleiros et al. (2010). Besides, considering the error bar, it also coincides with the temperature interval where feldspar BLG dominates (Borges and White, 1980; Simpson, 1998; Tullis, 2002), spanning the interval from ≈400°C to ≈600°C (Fig. 10A, B), and feldspar SGR starts to play a role between 500-550°C (Simpson, 1985; Gapais, 1989; Pryer, 1993).

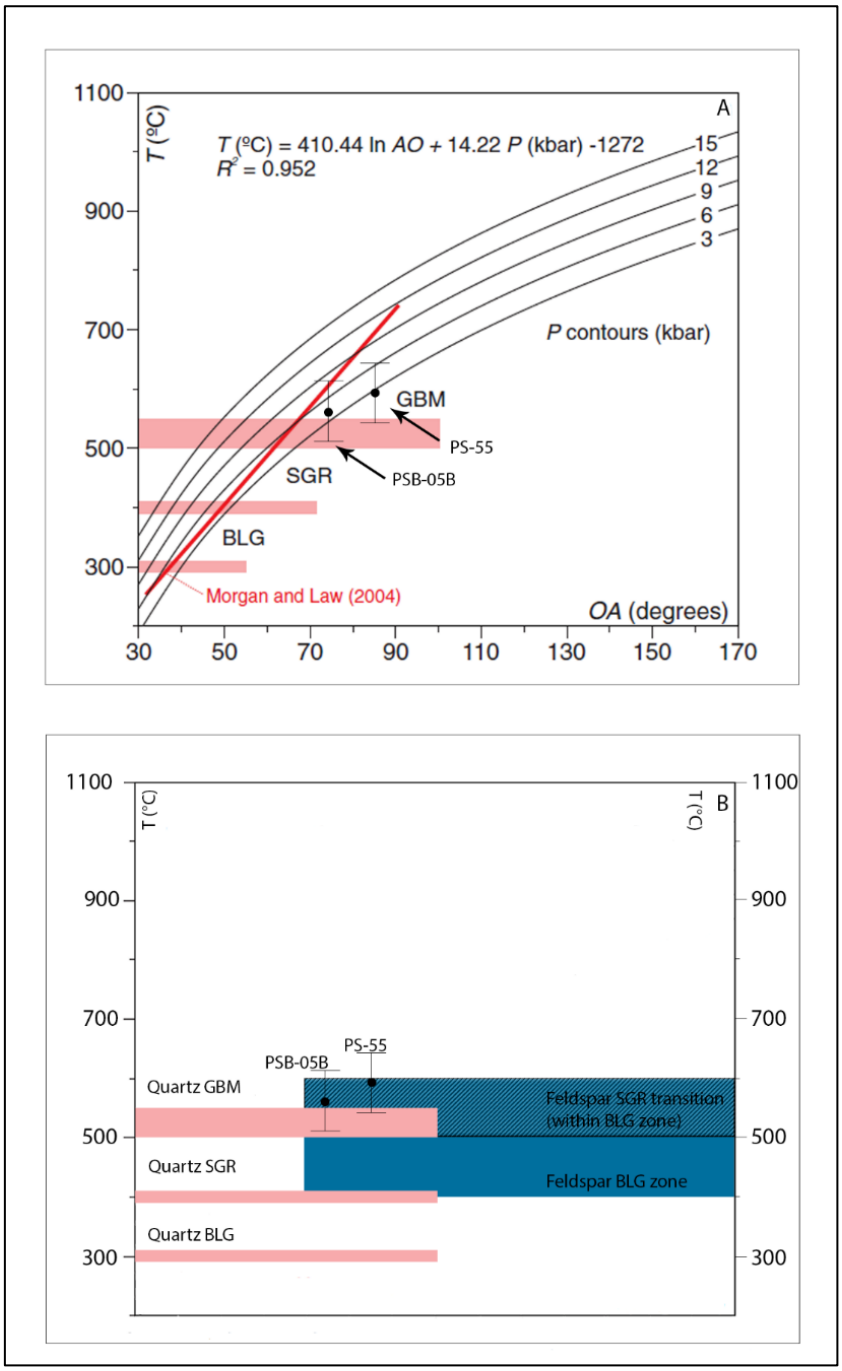

Figure 13. Samples PSB-05B and PS-55 plotted in (a) contour of opening-angle in the P-T field calculated using Faleiros et al. (2016) new calibration. The diagram presents transition zones (pink rectangles) between bulging (BLG), subgrain rotation (SGR) and grain boundary migration (GBM) according to Stipp et al. (2002 a, b) and Faleiros et al. (2010). Adapted from Faleiros et al. (2016); (b) Relationship between quartz dynamic recrystallization mechanisms (Stipp, 2002 a, b; Faleiros et al., 2010) and feldspar dynamic recrystallization of bulging (BLG; Borges and White, 1980; Simpson, 1998; Tullis, 2002) and subgrain rotation (SGR; Simpson, 1985; Gapais, 1989; Pryer, 1993).

6. VORTICITY ANALYSIS

Vorticity analysis of rocks naturally deformed displays an important measure of deformation non-coaxiality, being essential for kinematics studies of shear zones. The kinematic vorticity number (W_k), or mean vorticity number (W_m; Passchier, 1988) ranges from 0 for strict pure shear to 1 for strict simple shear and can be quantified by several methods at the mesoscopic and microscopic scale (e.g., Passchier, 1987, 1988; Passchier and Urai, 1988; Simpson and De Paor, 1993; Wallis, 1995; Faleiros et al., 2016).

In this study, the vorticity numbers were quantified using two methods: rigid porphyroclasts method (Passchier, 1987; Wallis, 1995) and the δ/β method (Wallis, 1995). Results are summarized in table 4.

6.1. Rigid porphyroclast method

Several authors propose that rotation of rigid objects (e.g. porphyroclasts) within a viscous matrix is dependent of several factors including viscosity and the degree of non-coaxiality (Passchier, 1987; Simpson and De Paor, 1993; Wallis, 1995).

In simple shear model, the porphyroclasts rotates continuous and synthetically in relation to the shear direction. In general shear model, however, not all rigid particles are free to rotate continuously and synthetically in relation to the shear direction. In this case, the porphyroclasts behavior is dependent of its shape ratio, initial orientation and vorticity number Wm (Ghosh and Ramberg, 1976; Passchier, 1987). The Wallis's plot (Wallis, 1995) establishes the values of shape ratio (Rc) below which the objects rotate continuously. This value is then used to calculate Wm using the equation (3) (Wallis et al., 1993).

$$W_m^{RP} = \frac{Rc^2-1}{Rc^2+1} \quad (3)$$

Feldspar porphyroclasts were manually digitized using Adobe Illustrator® with 150-200 grains per sample to ensure a sound statistical representation and analysed using SPO2003 (Launeau and Robin, 2003).

6.2. δ/β – method

Quartz aggregates dynamically recrystallized commonly develop oblique foliation in relation to the kinematic flow direction (Lister and Snoke, 1984; Trullenque et al., 2006; Xypolias, 2010; Faleiros et al., 2016). This preferred orientation of new grains is interpreted as the result of a complex continuous nucleation process, passive deformation and rotation of recrystallized grains (Means, 1981).

This methods assumes that the major axis of recrystallized grains that forms the oblique foliation determines the instantaneous stretching axis (ISA) (Wallis, 1995). Besides, it assumes that the centre girdle of quartz CPO (β) is near orthogonal to the flow plane and the angle

between the mylonitic foliation and the direction perpendicular to the centre girdle is equal to the angle between the flow and flattening planes of the finite strain (Wallis, 1995; Faleiros et al., 2016).

The $W_m^{\delta/\beta}$ can be estimated by equation (4) (Wallis, 1995) through relation between the maximum angle (δ) between oblique and main foliation in combination with the angle (β) between the shear plane and principal foliation determined through quartz [c] axis fabric (Xypolias, 2010)

$$W_m^{\delta/\beta} = \sin 2(\delta + \beta) \quad (4)$$

The measurements of β angles were carried out through a MTEX code developed in MATLAB environmental which estimate the vorticity plane based on the difference the foliation plane (E-W) and the plane perpendicular to the orientation defined by the c-axis maxima. This process enables to estimate the vorticity angle (β) even without data in the centre girdle. The angle δ between oblique and mylonitic foliation, on the other hand, were carried out through petrographic analysis.

6.3. Results

The vorticity analysis though RP method result in W^{RP}_m ranging 0.43-0.70 (i.e. 50-70% of pure shear contribution). Results from δ/β method, on the other hand, indicate $W^{\delta/\beta}_m$ range which spans 0.85-0.99 (i.e. 65-99% of simple shear contribution) and three samples with $W^{\delta/\beta}_m$ ranging 0.24-0.47 (i.e. 68-80% of pure shear) marking the variety in vorticity towards the strike of the shear zone. It is clear that RP method presents similar range of values of W^{RP}_m to all samples (Fig. 12) and lower values in relation with $W^{\delta/\beta}_m$. The observed differences between both methods results are described in Faleiros et al. (2016), Law et al. (2004) and Xypolias (2010) for rock naturally deformed.

Stahr and Law (2011) developed a numerical modelling to comprehend the effects of variable finite strain on development of the orientation of rigid clasts (e.g. feldspar porphyroclasts) for distinct general shear flows. They suggest that most general shear flows developed under moderate-high strain tend to produce clasts orientations with similar critical shape ratio (Rc) that might suggest similar contributions of pure and simple shear contributions (Wm ≈ 0.71). Based in numerical modelling (Stahr and Law, 2014) and observations of rocks naturally deformed in Faleiros et al. (2016), Law et al. (2004) and Xypolias (2010), Wm estimates through δ/β method are more reliable for Taxaquara Shear Zone which suggest variation between pure and simple shear contribution towards the strike of the shear zone.

7. QUARTZ PALEOPIEZOMETRY

Quartz correspond to one of the most abundant mineral phase within the continental crust and its dislocation creep microstructures are useful to understand deformation conditions in the mid to deep crust (Dunlap et al., 1997; Stipp et al., 2002a; Faleiros et al., 2010, 2016). These dislocation creep tend to gather into planar walls subdividing grains into subgrains, steady state feature of the substructure (Twiss, 1997), and its size is function of the applied differential stress. The fundamental assumption of this theory is that the formation of new grains through recrystallization processes must be energetically favorable (Twiss, 1997).

Paleopiezometers consist in a calibration related with diameter of new grains (subgrains) originated through recrystallization processes and stress flow (equal to differential stress) being proposed by several authors in the last four decades. Mercier et al. (1977), Christie et al. (1980) and Koch (1983) proposed paleopiezometers for quartz based on experiments. However, they usually overestimate the stress flow due its poor stress resolution and no distinguishing different mechanisms of dynamic recrystallization to quartz giving unrealistic stress flow predictions when extrapolated to natural shear zones conditions (Stipp and Tullis, 2003; Stipp et al., 2002b).

Recently, Stipp and Tullis (2003) proposed a recrystallized grain size paleopiezometer for quartz based on its mechanisms of dynamic recrystallization, especially regimes 2 (SGR) and 3 (combination of SGR and GBM) of Hirth and Tullis (1992). As shown before, quartz grain statistics (Fig. 6; table 3) and microstructural evidences (Fig. 7; table 2) suggest that all samples along the strike of TSZ were affected by SGR with small GBM contribution. Thus, this work focused on Stipp and Tullis (2003) piezometer due similarities in mechanisms of dynamic recrystallization for quartz and on theoretical piezometer relation of Twiss (1977) to derive differential stress and compare results between these two calibrations. Results are summarized in table 5.

7.1. Results

The results from Stipp and Tullis (2003) and Twiss (1997) paleopiezometers consist in a regular stress flow, with small data amplitude, to all samples towards the strike of the shear zone (Fig. 13) with 28.5 ± 2.5 MPa and 41.4 ± 3.2 MPa mean stress flow, respectively. Although both results indicate this regularity, they also show a gap between the values. This difference is present in Stipp and Tullis (2003, figure 4) where Twiss (1997) calibration plots above their paleopiezometer calibration and might be because the author does not consider the quartz mechanisms of dynamic recrystallization.

An important assumption on paleopiezometry studies is that the activated deformation mechanisms operative during the natural mylonitization and experimental deformation were the same (Hacker et al., 1992). Hence, quartz grain statistics and microstructural evidences

have demonstrated the importance of regime 2 and regime 3 (Hirth and Tullis, 1992) which is aligned with Stipp and Tullis (2003) piezometer. Based on this calibration, the results suggest an estimative of differential stress (σ_1- σ_3) varying from ≈20 MPa to ≈38 MPa with average ≈28.5 ± 2.5 MPa to TSZ in the study area.

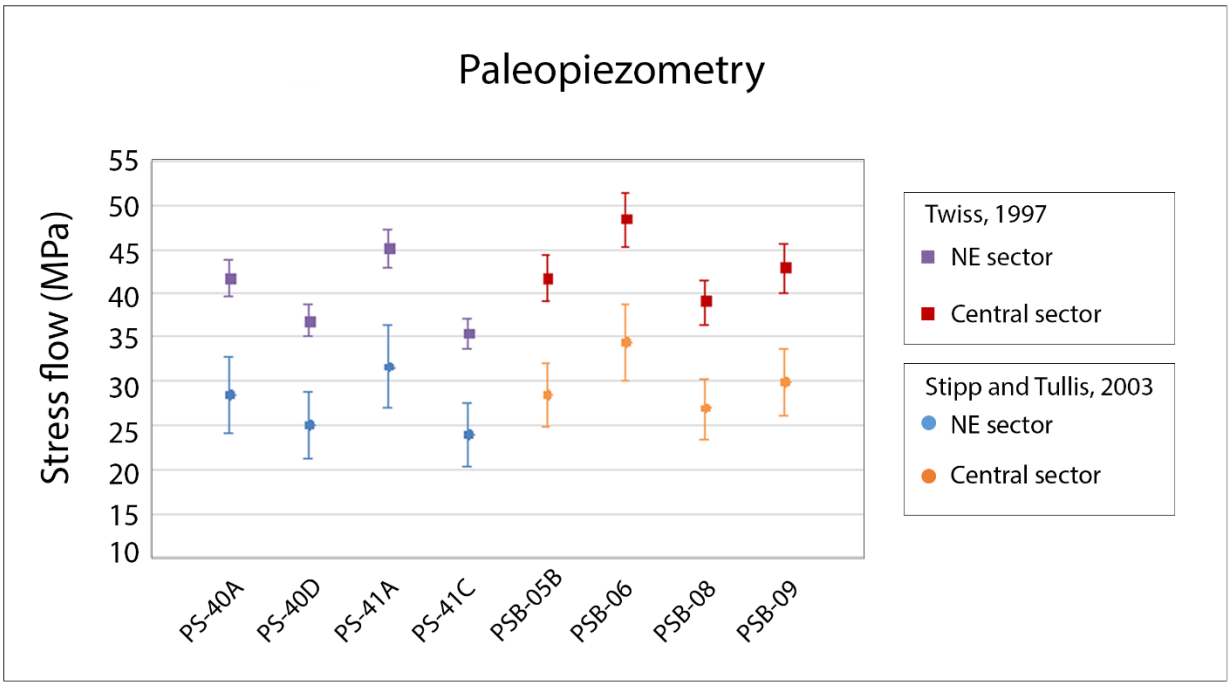

Figure 14. Paleopiezometry based on Twiss (1997) and Stipp and Tullis (2003) based on quartz Feret diameter (µm) and its mechanisms of recrystallization.

8. ESTIMATES OF STRAIN RATE AND QUARTZ VISCOSITY

Temperature, strain rate and fluid activity are the most important factor that influences the mechanisms of dynamic recrystallization for quartz (Faleiros et al., 2010) and a relation between strain rate and differences in the temperatures of distinguished recrystallization mechanisms is suggested by Stipp et al. (2002b).

Measured grain sizes and estimated differential stress and deformation temperature were used to evaluate strain rate by using “flows law” (Eq. 5) derived from laboratory experiments that can be useful to predict an unknown variable (temperature, differential stress, strain rate).

$$\dot{\varepsilon} = A\Delta\sigma^{n} f_{H20}^{m} \cdot \exp(-\frac{Q}{RT}) \quad (5)$$

where A = material constant ($MPA^{-n}\ s^{-1}$); $\Delta\sigma$ = differential stress (MPa); f = water fugacity; Q = creep activation energy (kJ/mol^{-1}); R = Clapeyron constant; T = temperature (K); n = stress exponent; m = water fugacity exponent; $\dot{\varepsilon}$ = strain rate (s^{-1}).

In this paper, strain rate was estimated from Luan and Paterson (1992), Brodie and Rutter (2000) and Hirth et al. (2001) parameters for wet quartz using a temperature and a differential stress interval which spans 500-600°C and 20-40 MPa, respectively. Strain rate values were evaluated between 500-550°C and 25-35 MPa given the intervals previously determined. Differential stress of 20 MPa and 40 MPa were plotted as boundary conditions. This estimate does not consider water fugacity due the absence mineral paragenesis that could indicate lithostatic pressure.

8.1. Results

Considering that the deformation temperature spans ≈500-550°C, mean differential stress is ≈28.5 ± 2.5 MPa, despite slightly differences between calibrations for wet quartz (Luan and Paterson, 1992; Brodie and Rutter, 2000; Hirth et al., 2001), they suggest an estimated strain rate yielding 10^{-14}-10^{-13} s^{-1} to differential stress range between 25-35MPa (Fig. 14, black rectangles). Thus, quartz viscosity can be quickly calculated though relation between differential stress and strain rate (Eq. 6).

$$\eta = \frac{\Delta\sigma}{\dot{\varepsilon}} \quad (6)$$

where η = viscosity (Pas).

Considering the same interval to temperature and differential stress, the calibrations suggest a quartz viscosity interval yielding 10^{21}-10^{22} Pas (Fig. 14).

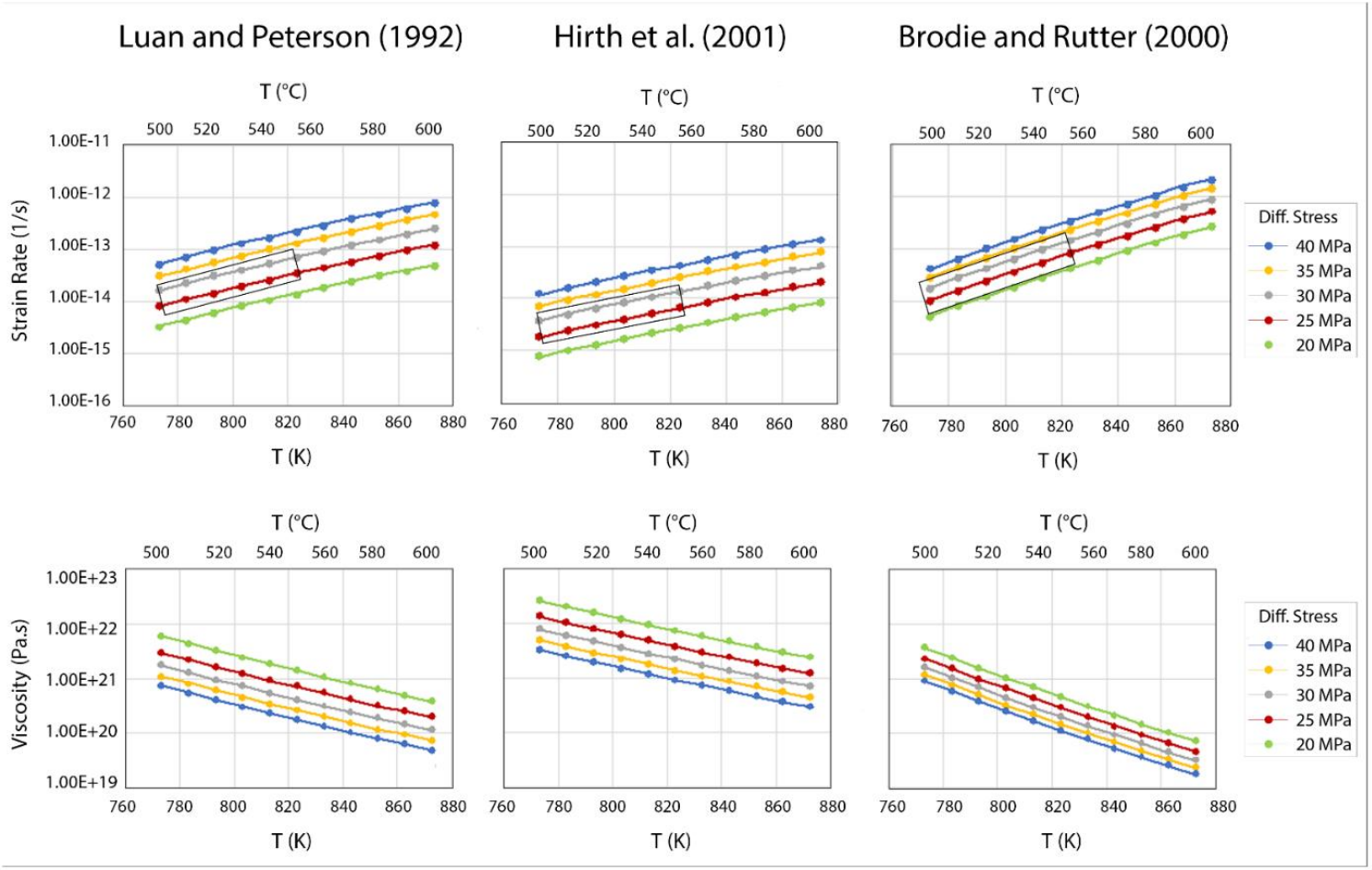

Figure 15. Estimate of strain rate and quartz viscosity based on Luan and Peterson (1992), Hirth et al. (2001), Brodie and Rutter (2000) with deformation temperature interval between 500-600°C and differential stress varying from 20 MPa to 40 MPa. Black rectangles indicate the most reliable values to TSZ (500-550°C, 25-35 MPa).

9. DISCUSSION

9.1. Transpressional regime

The NE-trending dextral Taxaquara Shear Zone, parallel to Ribeira belt structural trend, has a mean stretching lineation gently plunging NE. However, in detail, lineations are scattered distributed along a 90° section of the main shear plane, suggesting either a variety of local transport directions or the possibility that deformation was a result of transpression. Steeply-plunging lineation related to a transpressional shear zone was first described in the Canadian shield (Hudleston et al., 1988; Bauer and Bidwell, 1990).

Robin and Cruden (1994) developed a dynamical model of stress and strain distribution to investigate its and vorticity patterns in ideally ductile vertical transpression zone in which the material within the zone, modelled as linearly viscous, does not slip freely along the wall. Using the principle of superposition of two rheological solution to two boundary-value problems, they modelled the extrusion of the material related to the 'press' component, and the shearing parallel to the wall of the zone related to the 'trans' component of the motion. Beyond other results, the authors propose that plunge variations of stretching lineation within a single shear zone, varying from sub-horizontal to vertical, are strongly dependent on the magnitude of the 'press' over 'trans' component (i.e., the ratio between pure and simple shear) controlled by transpression regime. The predictions of the model are in good agreement with the examples mentioned by them (Larder Lake-Cadillac deformation zone, Canada; 'Mylonite zone' within the Mid-Proterozoic Sveconorwegian orogenic province, Sweden). Steeply-plunging stretching lineation, and thus the orientation of the long axis of the finite strain ellipsoid, are also proposed as a result of theoretical modeling of homogeneous transpressional shear zone by Sanderson and Marchini (1984), Fossen and Tikoff (1993), Fossen et al. (1994) and Tikoff and Teyssier (1994).

Different vorticity patterns, and thus different contributions of pure and simple shear, are observed in quartz crystallographic preferred orientation (CPO) and vorticity analysis. Samples from NE sector of TSZ display a regular symmetrical to slightly asymmetrical geometry towards Y axis, with dextral shear sense, suggesting a single girdle pattern and, therefore, more important simple shear compared with pure shear. Samples from Central sector, on the other hand, present diffuse patterns with two orthorhombic and three monoclinic symmetries. The presence of orthorhombic and monoclinic symmetries suggests different contribution of pure and simple shear towards

the strike of TSZ. The different contributions of simple and pure shear toward the shear zone is also confirmed by vorticity analysis.

Thus, the distribution of stretching lineation varying from sub-horizontal to oblique with vertical mylonitic foliation and vorticity variations (i.e. different contribution of pure and simple shear) towards the strike of TSZ argues in good agreement with a transpressive regime with predominant simple over pure shear ("press component"). This tectonic regime which is also described as the main regional regime based on field-based information (Machado and Endo, 1993; Hackspacher and Godoy, 1998; Dantas et al., 2000; Egydio-Silva et al., 2002) through regional strucutres such as subvertical transposition foliations, strain partitioning between coeval and subparallel fold, ductile thrusts and strike-slip shear zones accommodating large orogen-parallel movements and shortening (Ebert and Hasui, 1992; Ebert et al., 1996) and quantitative analyzes through strain analysis (Fiori, 1985; Ebert et al. 1996; Campanha and Sadowski, 2002; Faleiros et al., 2016).

9.2. Estimates of deformation temperature

The microstructures, together with the mineral paragenesis help constrain the deformation temperature. The dominance of SGR concomitant with minor GBM suggest a deformation temperature between ≈420-550ºC for quartz (Stipp et al., 2002; Faleiros et al., 2010). Evidence for bulging is minor and interpreted as final stages of recrystallization during exhumation of the TSZ decreasing temperature. The coexistence of brittle and ductile microstructures observed in feldspar porphyroclasts (Fig. 8) suggest a fluctuation in temperature around its brittle-ductile transition (≈450-500ºC, Tullis et al., 1982; Viegas et al., 2016; Fossen and Cavalcante, 2017). In normal conditions, these microstructures combine also suggest depth around 15-20 km situating these rocks at mid-continental crust conditions (Fossen and Cavalcante, 2017; figure 3).

This temperature interval inferred from the microstructures is consistent with the activated slip systems indicated by quartz CPO, where a strong contribution of 'basal-<a>' + 'rhomb-<a>' and 'rhomb-<a>' + 'prism-<a>' are observed in NE and Central sectors, respectively, which are activated in medium temperature (400-500°C; Passchier and Trouw, 2005). The opening-angle thermometer (T_{OA}) used in the two samples above and yielding T_{OA} of ≈512-646ºC, considering error bars, provide a deformation temperature interval which spans SRG and GBM transition for quartz and coincides with BLG zone and SGR transition zone (fig. 11). Deformation temperature above 550°C are unlikely given that GBM would be the predominant mechanism of dynamical

recrystallization for quartz and it is not observed. Hence, the T_{OA} interval must be critically interpreted (Faleiros et al., 2016; Hunter, 2017).

The consolidation of microstructural and opening-angle thermometer data establishes a deformation temperature interval yielding ≈500-550ºC suggesting mylonitization under upper greenschist metamorphic facies conditions in accordance with the mineral assemblage composed of quartz + alkali feldspar + plagioclase + biotite + muscovite + epidote present in nearly all samples. Quartz grain statistics (Fig. 6) and microstructural analysis indicates that all samples, both along and across the strike of TSZ, were deformed at the same metamorphic condition and recrystallized preferentially by subgrain rotation within biotite metamorphic zone., with minor contribution of grain boundary migration.

9.3. Comparison with Ribeira Shear Zone

Similar to the TSZ, the NE-trending Ribeira Shear Zone (RSZ) is a major dextral strike-slip structure within the Ribeira belt that was active during the Neoproterozoic Brasiliano-Pan African Orogeny and its deformation, differential stress and strain rate conditions were investigated by Faleiros et al. (2010). Based on quartz microstructural, opening-angle thermometer and geothermobarometry analysis, the authors distinguished different temperature intervals for distinct mechanisms of dynamic recrystallization where BLG plays a role between 400-420°C (chlorite zone), SGR in the range of 470-490°C (biotite zone) and GBM above 540°C (garnet zone). Using the paleopiezometer calibration proposed by Twiss (1977) for the grain boundary migration regime and by Stipp and Tullis (2003) for bulging, and subgrain rotation mechanisms, Faleiros et al. (2010) estimated differential stress for the Ribeira Shear Zone ranging from 87-143 MPa for BLG samples, 30-64 MPa for SGR samples and 15-25 MPa for GBM samples. The estimates for BLG samples in Faleiros et al. (2010) should be cautiously observed once Stipp and Tullis (2003) paleopiezometer is calibrated to regime 2 (SGR) and regime 3 (concomitant SGR and GBM) of Hirth and Tullis (1992). Strain rate estimated by flow laws with Hirth et al. (2001) parameters for wet quartz and water fugacity calculated at 600 MPa (Tödheide, 1972) indicates an average of $\approx 10^{-12}$ s^{-1}.

As shown above, the TSZ samples are dominated by SGR within biotite metamorphic zone possibly at slightly higher T than those for the RSZ. The results yielded a wider range of strain rates at lower values (10^{-13}-10^{-15} s^{-1}) without consider water fugacity (F_{H2O}), due to the lack of information about pressure conditions. Without F_{H2O}, higher values of strain rate are estimated at higher temperatures (Fig. 14). In the TSZ case, temperatures above 550ºC are not observed suggesting that an average strain rate of $\approx 10^{-12}$ s^{-1} is not

likely to occur. However, considering similar pressure and water fugacity conditions used in Faleiros et al. (2010), the strain rate for the TSZ increases to an average ≈10^{-12} s^{-1} for Hirth et al. (2001) calibration. It suggests that water fugacity allows higher strain rates to occur in lower temperatures and reduce the range amplitude considering the same differential stress interval (25 – 35 MPa). Both TSZ and RSZ zones belong to the same tectonic context and since a positive correlation regarding deformation conditions (i.e. deformation temperature and metamorphic condition) and microstructures was established, it is reasonable to assume same condition of pressure of 600 MPa and, therefore, water fugacity. Besides, the presence of biotite and epidote indicates the presence of water during deformation process.

Despite small differences, that can be considered insignificant in view of the uncertainties in the experimental data and the extrapolations involved (Hacker et al., 1992), both Taxaquara and Ribeira Shear Zones present information which allow a good data correlation between these major structures with ≈200 km distance from each other. Quartz-rich rocks are strength-controlling in plastic deformation above about 15 km (Ord and Hobbes, 1989), thus the data integration from Taxaquara and Ribeira Shear Zones can provide valuable information about the rheology of continental crust in Ribeira belt deformed with an average strain rate ≈10^{-12} s^{-1} and average quartz viscosity 10^{18}-10^{19} Pas. However, microscale and quantitative studies need to be expanded to others shear zones within the Ribeira belt to establish a good data set and generate a proper rheological model of continental crust evolution.

10. CONCLUSIONS

Our results allow to infer the deformation mechanisms, temperature, vorticity, flow stress, strain rate and viscosity prevailing during the deformation of the Taxaquara Shear Zone mylonites.

Quartz CPOs present different patterns varying from monoclinic to orthorhombic geometries which is suggestive of variations between pure and simple shear contribution. Vorticity results through rigid porphyroclast method suggest similar mean vorticity number for all analysed samples (Fig. 12, 0.43-0.70) which indicates medium to high finite strain conditions according to numerical models (Stahr and Law, 2014). However, results from δ/β method suggest mean vorticity number with contribution of pure (0.24-0.47) and simple shear (0.85-0.99). Thus, this vorticity variation associated with structural setting (vertical foliation and sub-horizontal to oblique lineation) agree with transpressional models (Sanderson and Marchini, 1984; Robin and Cruden, 1994; Tikoff and Greene, 1997). This regime is in a good agreement with that already proposed (Ebert and Hasui, 1992; Machado and Endo, 1993; Ebert et al., 1996; Dantas et al., 2000; Egydio-Silva et al., 2002) and quantified though strain analysis (Fiori, 1985; Ebert et al. 1996; Campanha and Sadowski, 2002; Faleiros et al., 2016) to Ribeira belt.

The mylonitization of granitic rocks affected by TSZ occurred under upper greenschist metamorphic facies within biotite zone with deformation temperature around 500-550°C based on quartz and feldspar microstructures (SGR ± GBM for quartz and BLG ± SGR for feldspar), matrix mineral assemblage (quartz + feldspar + biotite + muscovite ± epidote), quartz slip systems and opening-angle thermometer. These results allows a good correlation with Ribeira Shear Zone (Faleiros et al., 2010) with also similar stress flow estimates to SGR samples (25-35 MPa) and strain rate (≈10-12 s-1) placing both structure in mid-continental crust level. It shows the importance detailed studies of shear zones within Ribeira belt to establish regional correlations and to comprehend the rheology of continental crust during Brazilian-Pan African Orogeny.

11. REFERENCES

Almeida, F.F.M., Amaral, G., Cordani, U., Kawashita, K., 1973. The Precambrian evolution of the South American Cratonic Margin, South of Amazon River. The Ocean Basin and Margins. New York Plenum, 411–416.

Borges, F.S., White, S.H., 1980. Microstructural and chemical studies of sheared anorthosites, Roneval, South Harris. *Journal of Structural Geology* 2, 273–280. https://doi.org/10.1016/0191-8141(80)90060-7

Brodie, K.H., Rutter, E.H., 2000. Deformation mechanisms and rheology: why marble is weaker than quartzite. *Journal of the Geological Society* 157, 1093–1096. https://doi.org/10.1144/jgs.157.6.1093

Campanha, G.A.C., 2002. *O papel do sistema de zonas de cisalhamento transcorrentes na configuração da porção meridional da Faixa Ribeira*. Tese (Livre Docência). São Paulo - Instituto de Geociências da Universidade de São Paulo.

Campanha, G.A.C., Basei, M.S., Faleiros, F.M., Nutman, A.P., 2016. The Mesoproterozoic to early Neoproterozoic passive margin Lajeado Group and Apiaí Gabbro, Southeastern Brazil. *Geoscience Frontiers* 7, 683–694. https://doi.org/10.1016/j.gsf.2015.08.004

Campanha, G.A.C., Brito Neves, B.B., 2004. Frontal and oblique tectonics in the Brazilian shield. *Episodes* 27, 255–259.

Campanha, G.A.C., Faleiros, F.M., Basei, M.A.S., Ribeiro, B.V., 2016. *Embu complex in its type area southwest of São Paulo*. 48 Geoscience Brazilian Congress.

Campanha, G.A.C., Faleiros, F.M., Basei, M.A.S., Tassinari, C.C.G., Nutman, A.P., Vasconcelos, P.M., 2015. Geochemistry and age of mafic rocks from the Votuverava Group, southern Ribeira Belt, Brazil: Evidence for 1490Ma oceanic back-arc magmatism. *Precambrian Research* 266, 530–550. https://doi.org/10.1016/j.precamres.2015.05.026

Campanha, G.A.C., Sadowski, G.R., 1999. Tectonics of the southern portion of the Ribeira Belt (Apiaí Domain). *Precambrian Research* 98, 31–51. https://doi.org/10.1016/S0301-9268(99)00027-3

Campos Neto, M.C., 2000. Orogenic system from southwestern Gondwana: an approach to brasilian-pan afrian cycle and orogenic collage in southeastern Brazil. *Tectonic Evolution of South America*. 335–365.

Dantas, E.L., Hackspacher, P.C., Fetter, A.H., Sato, K., Pimentel, M.M., Godoy, A.M., 2000. Nd Isotope Systematics Related To Proterozoic Evolution of the Central Ribeira Belt in the State of São Paulo, Se Brazil. *Revista Brasileira de Geociências* 30, 140–143.

Dell'angelo, L.N., Tullis, J., 1989. Fabric development in experimentally sheared quartzites. *Tectonophysics* 169, 1–21. https://doi.org/10.1016/0040-1951(89)90180-7

Dell'Angelo, L.N., Tullis, J., 1986. A comparison of quartz c-axis preferred orientations in experimentally deformed aplites and quartzites. *Journal of Structural Geology* 8, 683–692.

Ebert, H.D., Chemale, F., Babinski, M., Schmus, W.R. Van, 1996. Tectonic setting and U / Pb zircon dating of the plutonic Socorro Complex in the Transpressive. *Tectonics* 15(3), 688–699.

Ebert, H.D., Hasui, Y., 1992. Transpressive evolution of a collisional suture zone in SE-Brazil., 29th *International Geological Congress*.

Egydio-Silva, M., Vauchez, A., Bascou, J., Hippertt, J., 2002. High-temperature deformation in the Neoproterozoic transpressional Ribeira belt, southeast Brazil. *Tectonophysics* 352, 203–224. https://doi.org/10.1016/S0040-1951(02)00197-X

Etchecopar, A., 1977. A plane kinematic model of progressive deformation in a polycrystalline aggregate. *Tectonophysics* 39, 121–139. https://doi.org/10.1016/0040-1951(77)90092-0

Faleiros, F.M., Ademar, Campanha, G.A.C., Maria, R., Fuzikawa, K., 2010. Tectonophysics Quartz recrystallization regimes , c-axis texture transitions and fl uid inclusion reequilibration in a prograde greenschist to amphibolite facies mylonite zone (Ribeira Shear Zone, SE Brazil). *Tectonophysics* 485, 193–214. https://doi.org/10.1016/j.tecto.2009.12.014

Faleiros, F.M., Campanha, G.A.C., Martins, L., Vlach, S.R.F., Vasconcelos, P.M., 2011. Ediacaran high-pressure collision metamorphism and tectonics of the southern Ribeira Belt (SE Brazil): evidence for terrane accretion and dispersion during Gondwana assembly. *Precambrian Research* 189, 263–291.

Faleiros, F.M., Campanha, G.A.C., Pavan, M., Almeida, V. V., Rodrigues, S.W.O., Araújo, B.P., 2016. Short-lived polyphase deformation during crustal thickening and exhumation of a collisional orogen (Ribeira Belt, Brazil). *Journal of Structural Geology* 93, 106–130. https://doi.org/10.1016/j.jsg.2016.10.006

Faleiros, F.M., Moraes, R., Pavan, M., Campanha, G.A.C., 2016. Tectonophysics A new empirical calibration of the quartz c-axis fabric opening-angle deformation thermometer. *Tectonophysics* 671, 173–182. https://doi.org/10.1016/j.tecto.2016.01.014

Fedorov, E.S., 1982. Eine neue Methode der optischen Untersuchung von Krystallplatten in parallelem Lichte. *Tschermak's Mineralogische Und Petrographische Mittheilungen* 12, 505–509.

Fossen, H., Cavalcante, G.C.G., 2017. Shear zones – A review. *Earth-Science Reviews*. https://doi.org/10.1016/j.earscirev.2017.05.002

Fossen, H., Tikoff, B., 1993. The deformation matrix for simultaneous pure shear, simple shear, and volume change, and its application to tranpression/transtension tectonics. *Journal of Structural Geology* 15, 413–425.

Fossen, H., Tikoff, B., Teyssier, C., 1994. Strain modeling of transpressional and transtensional deformation. *Norsk Geologisk Tidsskrift* 74, 134–145.

Gapais, D., 1989. Shear structures within deformed granites: Mechanical and thermal indicators. *Geology* 17, 1144–1147.

Ghosh, S.K., Ramberg, H., 1976. Reorientation of inclusions by combination of pure shear and simple shear. *Tectonophysics* 34, 1–70. https://doi.org/10.1016/0040-1951(76)90176-1

Hacker, B.R., Yin, A., Christie, J.M., Davis, G.A., 1992. Stress magnitude, strain rate and rheology of extended middle continental crust inferred from quartz grain sizes in the Whipple Mountains, California. *Tectonics* 11, 36–46.

Hackspacher, P.C., Godoy, A.M., 1998. Vertical displacement during post-collisional escape tectonism (Brasiliano Orogeny) of the Ribeira Belt, Sao Paulo, Brazil. *Journal of African Earth Sciences* 27, 99–100.

Hasui, Y., 1975. Geologia da folha de são Roque. *Boletim IG*, Instituto de Geociências, USP 6, 157–183. https://doi.org/10.2307/1134315

Hasui, Y., 1973. *Tectônica da área das folhas de São Roque e Pilar do Sul*. Tese (Doutorado). São Paulo: Instituto de Geociências da Universidade de São Paulo

Hasui, Y., Carneiro, C.R., Coimbra, A.M., 1975. The Ribeira folded belt. *Revista Brasileira de Geociências* 5, 257–266.

Hasui, Y., Sadowski, G.R., 1976. Evolução geológica do Pré-Cambriano na região sudeste do Estado de São Paulo. *Revista Brasileira de Geociências* 6, 182–200.

Heilbron, M., Pedrosa-Soares, A.C., Campos Neto, M.D.C., Silva, L.D., Trouw, R.A.J., Janasi, V.D.A., 2004. Província Mantiqueira. Geologia Do Continente Sul-Americano: Evolução Da Obra Ed Fernando Flávio Marques de Almeida. 203–235.

Heilbronner, R., Tullis, J., 2006. Evolution of c axis pole figures and grain size during dynamic recrystallization: Results from experimentally sheared quartzite. *Journal of Geophysical Research: Solid Earth* 111, 1–19. https://doi.org/10.1029/2005JB004194

Heilbronner, R., Tullis, J., 2002. The effect of static annealing on microstructures and crystallographic preferred orientations of quartzites experimentally deformed in axial compression and shear. *Geological Society, London, Special Publications* 200, 191–218. https://doi.org/10.1144/GSL.SP.2001.200.01.12

Hennies, W.T., Hasui, Y., Penalva, F., 1967. O falhamento transcorrente de Taxaquara. *Congresso Brasileiro de Geologia* 21.

Henrique-Pinto, R., Janasi, V.., Vasconcellos, A.C.B.C., Sawyer, E.W., Barnes, S.-J., Basei, M.A.S., Tassinari, C.C.G., 2015. Zircon provenance in meta-sandstones of the São Roque Domain: Implications for the Proterozoic evolution of the Ribeira Belt, SE Brazil. *Precambrian Research* 256.

Hirth, G., Teyssier, C., Dunlap, W.J., 2001. An evaluation of quartzite flow laws based on comparisons between experimentally and naturally deformed rocks. International *Journal of Earth Sciences* 90, 77–87. https://doi.org/10.1007/s005310000152

Hirth, G., Tullis, J., 1992. Dislocation creep regimes in quartz aggregates. *Journal of Structural Geology* 14, 145–159. https://doi.org/10.1016/0191-8141(92)90053-Y

Hunter, N.J.R., 2017. The anatomy of "hot-on-cold" shear zones : insights from quartzites of the Main Central Thrust in the Alaknanda region (Garhwal Himalaya). Thesis (PhD). Melbourne: Monash University.

Hunter, N.J.R., Wilson, C.J.L., Luzin, V., 2016. Comparison of quartz crystallographic preferred orientations identified with optical fabric analysis , electron backscatter and neutron diffraction techniques. *Journal of Microscopy* 265, 169–184. https://doi.org/10.1111/jmi.12472

Janasi, V.., Leite, R.., van Schmus, W.., 2001. U–Pb chronostratigraphy of the granitic magmatism in the Agudos Grandes Batholith (west of São Paulo, Brazil) — implications for the evolution of the Ribeira Belt. *Journal of South American Earth Sciences* 14, 363–376. https://doi.org/10.1016/S0895-9811(01)00034-7

Keller, L.M., Stipp, M., 2011. The single-slip hypothesis revisited: Crystal-preferred orientations of sheared quartz aggregates with increasing strain in nature and numerical simulation. *Journal of Structural Geology* 33, 1491–1500. https://doi.org/10.1016/j.jsg.2011.07.008

Kruhl, J.H., 1996. Prism- and basal-plane parallel subgrain boundaries in quartz: a microstructural geothermobaromether. *Journal of Metamorphic Geology* 14, 581–589. https://doi.org/10.1046/j.1525-1314.1996.00413.x

Launeau, P., Robin, P.Y.F., 2003. *SPO (software)*.

Law, R.D., 2014. Deformation thermometry based on quartz c -axis fabrics and recrystallization microstructures : A review. *Journal of Structural Geology* 66, 129–161. https://doi.org/10.1016/j.jsg.2014.05.023

Law, R.D., Searle, M.P., Simpson, R.L., 2004. Strain, deformation temperatures and vorticity of flow at the top of the Greater Himalayan Slab, Everest Massif, Tibet. *Journal of the Geological Society* 161, 305–320. https://doi.org/10.1144/0016-764903-047

Leite, R.., 1997. Geologia, petrografia e geoquıímica dos granitos da região de Piedade (SP). Tese (Mestrado). São Paulo: Instituto de Geociências da Universidade de São Paulo.

Leite, R.J., Heaman, L.M., de Assis Janasi, V., Martins, L., Creaser, R.A., 2007. The late- to postorogenic transition in the Neoproterozoic Agudos Grandes Granite Batholith (Apiaí Domain, SE Brazil): Constraints from geology, mineralogy, and U–Pb geochronology. *Journal of South American Earth Sciences* 23, 193–212. https://doi.org/10.1016/j.jsames.2006.09.022

Leite, R.J., Janasi, V.A., Martins, L., 2006. Contamination in mafic mineral-rich calc-alkaline granites: a geochemical and Sr-Nd isotope study of the Neoproterozoic Piedade Granite, SE Brazil. *Anais Da Academia Brasileira de Ciências* 78, 345–371. https://doi.org/10.1590/S0001-37652006000200013

Lister, G.S., 1977. Discussion: Crossed-girdle c-axis fabrics in quartzites plastically deformed by plane strain and progressive simple shear. *Tectonophysics* 39, 51–54. https://doi.org/10.1016/0040-1951(77)90087-7

Lister, G.S., Hobbs, B.E., 1980. The simulation of fabric development during plastic deformation and its application to quartzite : the influence of deformation history. *Journal of Structural Geology* 2, 355–370.

Lister, G.S., Snoke, A.W., 1984. S--C Mylonites. *Journal of Structural Geology* 6, 617–638.

Luan, F.C., Paterson, M.S., 1992. Preparation and deformation of synthetic aggregates of quartz. *Journal of Geophysical Research: Solid Earth* 97, 301–320.

Machado, R., Endo, I., 1993. Cinturão de cisalhamento atlântico: um exemplo de tectônica transpressional neoproterozoica., *Anais do IV simpósio nacional de estudos tectônicos* 189–191.

Martins, L., 2001. Condições de cristalização de granitos sin- e tardi-orogênicos da porção central do batólito Agudos Grandes, SP, com base em geoquıímica de minerais e rochas. Tese (Mestrado). São Paulo: Instituto de Geociências da Universidade de São Paulo.

Means, W.D., 1981. The concept of steady-state foliation. *Tectonophysics* 78, 179–199. https://doi.org/10.1016/0040-1951(81)90013-5

Morgan, S.S., Law, R.D., 2004. Unusual transition in quartzite dislocation creep regimes and crystal slip systems in the aureole of the Eureka Valley–Joshua Flat–Beer Creek pluton, California: a case for anhydrous conditions created by decarbonation reactions. *Tectonophysics* 384, 209–231. https://doi.org/10.1016/j.tecto.2004.03.016

Neumann, B., 2000. Texture development of recrystallised quartz polycrystals unravelled by orientation and misorientation characteristics. *Journal of Structural Geology* 22, 1695–1711. https://doi.org/10.1016/S0191-8141(00)00060-2

Oliot, E., Goncalves, P., Schulmann, K., Marquer, D., Lexa, O., 2014. Mid-crustal shear zone formation in granitic rocks: Constraints from quantitative textural and crystallographic preferred orientations analyses. *Tectonophysics* 612–613, 63–80. https://doi.org/10.1016/j.tecto.2013.11.032

Oriolo, S., Oyhantçabal, P., Heidelbach, F., Wemmer, K., Siegesmund, S., 2015. Structural evolution of the Sarandí del Yí Shear Zone, Uruguay: kinematics, deformation conditions and tectonic significance. *International Journal of Earth Sciences* 104, 1759–1777. https://doi.org/10.1007/s00531-015-1166-2

Passchier, C.W., 1988. The use of Mohr circles to describe non-coaxial progressive deformation. *Tectonophysics* 149, 323–338. https://doi.org/10.1016/0040-1951(88)90181-3

Passchier, C.W., 1987. Stable positions of rigid objects in non-coaxial flow-a study in vorticity analysis. *Journal of Structural Geology* 9, 679–690. https://doi.org/10.1016/0191-8141(87)90152-0

Passchier, C.W., Trouw, R.A.J., 2005. Microtectonics (book).

Passchier, C.W., Urai, J.L., 1988. Vorticity and strain analysis using Mohr diagrams. *Journal of Structural Geology* 10, 755–763. https://doi.org/10.1016/0191-8141(88)90082-X

Peternell, M., Hasalová, P., Wilson, C.J.L., Piazolo, S., Schulmann, K., 2010. Evaluating quartz crystallographic preferred orientations and the role of deformation partitioning using EBSD and fabric analyser techniques. *Journal of Structural Geology* 32, 803–817. https://doi.org/10.1016/j.jsg.2010.05.007

Pryer, L.L., 1993. Microstructures in feldspars from a major crustal thrust zone: the Grenville Front, Ontario, Canada. *Journal of Structural Geology* 15, 21–36.

Rahl, J.M., Skemer, P., 2016. Microstructural evolution and rheology of quartz in a mid-crustal shear zone. *Tectonophysics* 680, 129–139. https://doi.org/10.1016/j.tecto.2016.05.022

Robin, P.Y.F., Cruden, A.R., 1994. Strain and vorticity patterns in ideally ductile transpression zones. *Journal of Structural Geology* 16, 447–466. https://doi.org/10.1016/0191-8141(94)90090-6

Sanderson, D.J., Marchini, W.R.D., 1984. Transpression. *Journal of Structural Geology* 6, 449–458. https://doi.org/10.1016/0191-8141(84)90058-0

Schmid, E., Boas, W., 1935. Kristallplastizit.

Schmid, S.M., Casey, M., 1986. ANALYSIS OF SOME COMMONLY OBSERVED QUARTZ C-AXIS (A). Mineral and Rock Deformation: Laboratory Studies: The Paterson Volume, American Geophysical Union, Washington, D. C.

Simpson, C., 1998. Variation in relative recrystallized grain sizes of quarts and feldspar with deformation temperature. Fault-Related Rocks: A Photographic Atlas. 256–259.

Simpson, C., 1985. Deformation of granitic rocks across the brittle-ductile transition. *Journal of Structural Geology* 7, 503–511. https://doi.org/10.1016/0191-8141(85)90023-9

Simpson, C., De Paor, D.G., 1993. Strain and kinematic analysis in general shear zones. *Journal of Structural Geology* 15, 1–20.

Skrotzki, W., 1994. Defect structure and deformation mechanisms in naturally deformed augite and enstatite. *Tectonophysics* 229, 43–68.

Stahr, D.W., Law, R.D., 2014. Strain memory of 2D and 3D rigid inclusion populations in viscous flows - What is clast SPO telling us? *Journal of Structural Geology* 68, 347–363. https://doi.org/10.1016/j.jsg.2014.05.028

Stahr, D.W., Law, R.D., 2011. Effect of finite strain on clast-based vorticity gauges. *Journal of Structural Geology* 33, 1178–1192. https://doi.org/10.1016/j.jsg.2011.05.002

Stipp, M., Holger, S., Heilbronner, R., Schmid, S.M., 2002a. The eastern Tonale fault zone : a "natural laboratory" for crystal plastic deformation of quartz over a temperature range from 250 to 700 8 C. *Journal of Structural Geology* 24, 1861–1884.

Stipp, M., Stünitz, H., Heilbronner, R., Schmid, S.M., 2002b. Dynamic recrystallization of quartz: correlation between natural and experimental conditions. Geological Society, London, Special Publications 200, 171 LP-190.

Stipp, M., Tullis, J., 2003. The recrystallized grain size piezometer for quartz. *Geophysical Research Letters* 30, 2088. https://doi.org/10.1002/2017GL073836

Stipp, M., Tullis, J., 2003. The recrystallized grain size piezometer for quartz, *Geophysical Research Letters*. https://doi.org/10.1029/2003GL018444

Stipp, M., Tullis, J., Scherwath, M., Behrmann, J.H., 2010. A new perspective on paleopiezometry: Dynamically recrystallized grain size distributions indicate mechanism changes. *Geology* 38, 759–762.

Tikoff, B., Greene, D., 1997. Stretching lineations in transpressional shear zones: an example from the Sierra Nevada Batholith, California. *Journal of Structural Geology* 19, 29–39. https://doi.org/10.1016/S0191-8141(96)00056-9

Tikoff, B., Teyssier, C., 1994. Strain modeling of displacement-field partitioning in transpressional orogens. *Journal of Structural Geology* 16, 1575–1588.

Tödheide, K., 1972. Water at high temperatures and pressures. The Physics and Physical Chemistry of Water. Springer New York, 463–514.

Toy, V.G., Prior, D.J., Norris, R.J., 2008. Quartz fabrics in the Alpine Fault mylonites : Influence of pre-existing preferred orientations on fabric development during progressive uplift. *Journal of Structural Geology* 30, 602–621. https://doi.org/10.1016/j.jsg.2008.01.001

Trouw, R.A.J., Passchier, C.W., 2010. Atlas of mylonites and related microstructures (book).

Trullenque, G., Kunze, K., Heilbronner, R., Stünitz, H., Schmid, S.M., 2006. Microfabrics of calcite ultramylonites as records of coaxial and non-coaxial deformation kinematics: Examples from the Rocher de l'Yret shear zone (Western Alps). *Tectonophysics* 424, 69–97. https://doi.org/10.1016/j.tecto.2006.06.004

Tullis, J., 2002. Deformation of Granitic Rocks: Experimental Studies and Natural Examples. *Reviews in Mineralogy and Geochemistry* 51, 51–95. https://doi.org/10.2138/gsrmg.51.1.51

Tullis, J., Snoke, A.W., Todd, V.R., 1982. Significance and petrogenesis of mylonitic rocks. *Geology* 10, 227–230.

Tullis, J., Yund, R.A., 1977. Experimental deformation of dry Westerly granite. *Journal of Geophysical Research* 82, 5705–5718.

Twiss, R.J., 1977. Theory and applicability of a recrystallized grain size paleopiezometer. *Stress in the Earth*. 227–244.

Viegas, G., Menegon, L., Archanjo, C.., 2016. Brittle grain-size reduction of feldspar, phase mixing and strain localization in granitoids at mid-crustal conditions (Pernambuco shear zone, NE Brazil). *Solid Earth* 7, 1–22.

Wallis, S., 1995. Vorticity analysis and recognition of ductile extension in the Sanbagawa belt, SW Japan., *Journal of Structural Geology*. https://doi.org/10.1016/0191-8141(95)00005-X

Wallis, S.., 1992. Vorticity analysis in a metachert from the Sanbagawa Belt, SW Japan. *Journal of Structural Geology* 14, 271–280. https://doi.org/10.1016/0191-8141(92)90085-B

Wallis, S.R., Platt, J.P., Knott, S.D., 1993. Recognition of syn-convergence extension in accretionary wedges with examples from the Calabrian Arc and the eastern Alps., *American Journal of Science*. https://doi.org/10.2475/ajs.293.5.463

Wheeler, J., Prior, D., Jiang, Z., Spiess, R., Trimby, P., 2001. The petrological significance of misorientations between grains. *Contributions to Mineralogy and Petrology* 141, 109–124. https://doi.org/10.1007/s004100000225

Wilson, C.J.L., Russell-Head, D.S., Kunze, K., Viola, G., 2007. The analysis of quartz c-axis fabrics using a modified optical microscope. *Journal of Microscopy* 227, 30–41. https://doi.org/10.1111/j.1365-2818.2007.01784.x

Xypolias, P., 2010. Vorticity analysis in shear zones: A review of methods and applications. *Journal of Structural Geology* 32, 2072–2092. https://doi.org/10.1016/j.jsg.2010.08.009

12. APPENDIX

Table 1. Mineral assembly and mylonites sample classification in Trouw et al. (2009).

Sample	Mylonite Classification *Trouw et al. 2009*	Mineralogical Assembly		
		General	Matrix	Minor Amounts
NE Sector				
PS - 41 B	Mylonite Medium grade	Pl (25%), Afs (20%), Qz (15%)	Bt + Fsp + Hbl (40%)	Op, Ap
PS - 41 C	Mylonite Medium grade	Fsp (15%), Qz (25%)	Bt + Fsp + Ms (60%)	Op, Ap
PS - 40 D	Protomylonite Medium grade	Qz (35%); Pl (15%), Afs (15%), Ms (15%)	Qz + Fsp (20%)	Tur, Grt, Ap
PS - 40 A	Mylonite Medium grade	Qz (15%), Ms (20%); Afs (10%), Pl (5%)	Bt + Ms (50%)	Ap
PS - 40 B	Protomylonite Medium grade	Qz (30%); Pl (20%); Afs (2%); Ap (4%); Op (3%); Ep (1%)	Bt + Ms + Hbl (40%)	Ap, Ep, Op
PS - 41 A	Mylonite Medium grade	Qz (20%); Pl (7%); Afs (13%);	Qz + Fsp + Bt + Ms + Hbl (60%)	Ap, Op
PS - 42 A	Mylonite Medium grade	Qz (25%); Afs (15%); Pl (10%);	Qz + Fsp + Bt + Ms (50%)	Tit, Ap, Op, Ep
PS - 42 B	Mylonite Medium grade	Qz (15%); Afs (15%); Pl (10%); Chl (5%); Ms (10%)	Qz + Fsp + Ms + Bt (45%)	Ap, Op, Cal
Central Sector				
P S - 55	Mylonite Medium grade	Qz (15%); Afs (15%); Pl (10%)	Qz + Fsp + Bt + Ms (60%)	Op, Tit, Ap
PSB - 05B	Protomylonite Medium grade	Qz (30%), Pl (25%), Afs (15%)	Qz + Fsp + Ms + Bt (30%)	Op, Ep, Ser
PSB - 06	Protomylonite Medium grade	Qz (30%), Pl (20%), Afs (20%), Tur (10%)	Qz + Fsp + Ms + Bt (20%)	Op, Ser
PSB - 08	Mylonite Medium grade	Qz (20%); Afs (15%); Pl (15%)	Qz + Fsp + Bt + Ms (50%)	Op, Ser
PSB - 09	Mylonite Medium grade	Qz (25%); Afs (10%); Pl (15%)	Qz + Fsp + Bt + Ms (50%)	Op, Ep, Ser

Ap: apatite; Bt: biotite; Ep: epidote; Afs: alkali feldspar; Fsp: feldspar (general); Hbl: hornblend; Op: opaque; Qz: quartz; Ser: sericite; Tit: titanite; Zr: zircon

Table 2. Kinematic and microstructural characterization based on quartz and feldspar deformation to establish a relationship with deformation processes and deformation temperature based on Stipp et al. (2002a).

Sample	Kinematic Indicators	Feldspar Deformation	Quartz Recrystallization	Estimated Temperature (°C) *Stipp et al. (2002a)*
NE Sector				
PS - 41 B	Non-oriented sample	Fracturing BLG Twinning deformation Pertites flame	Static, GBM, SGR	≈ 450 - 500
PS - 41 C	Non-oriented sample	Fracturing BLG Twinning deformation	GBM, SGR	≈ 450 - 500
PS - 40 D	Non-oriented sample	Fracturing BLG Twinning deformation	GBM, SGR	≈ 450
PS - 40 A	Muscovite *fish* Quartz oblique foliation S/C foliations Porphyroclasts type-σ & type-δ Clockwise rotation	SGR BLG Twinning deformation Undulose extionction	GBM, SGR	≈ 450 - 500
PS - 40 B	Muscovite fish Quartz oblique foliation S/C foliation Porphyroclasts type-σ & type-δ Clockwise rotation	Fracturing SGR BLG Undulose extinction	GBM, SGR	≈ 450
PS - 41 A	Quartz oblique foliation Porphyroclasts type-σ Clockwise rotation	Fracturing BLG Undulose extinction	GBM, SGR	≈ 450 - 550
PS - 42 A	Quartz oblique foliation S/C foliations marked by oblique biotite Porphyroclasts type-σ Clockwise rotation	SGR BLG Twinning deformation Undulose extionction	GBM, SGR	≈ 450 - 500
PS - 42 B	Quartz oblique foliation S/C foliations marked by oblique biotite Porphyroclasts type-σ Clockwise rotation	Fractuging SGR (less frequent) BLG Undulose extinction	GBM, SGR	≈ 450 - 500

Central Sector				
P S - 55	Quartz oblique foliation S/C foliations marked by oblique biotite Porphyroclasts type-σ Clockwise rotation	Fracturing SGR (less frequent) BLG Undulose extinction	Static, GBM, SGR	≈ 450 - 500
PSB - 05B	Quartz oblique foliation Sigmoidal quartz ribbons Muscovite fish Clockwise rotation	Fracturing BLG Twinning deformation Undulose extionction Pertites flame	Static, GBM, SGR	≈ 450 - 500
PSB - 06	Quartz oblique foliation S/C foliations marked by oblique biotite Clockwise rotation	Fracturing BLG Twinning deformation Undulose extionction Pertites flame	Static, GBM, SGR	≈ 450 - 500
PSB - 08	Porphyroclasts type-σ Clockwise rotation	Fracturing BLG Undulose extinction	GBM, SGR	≈ 450 - 500
PSB - 09	Sigmoidal quartz ribbons Porphyroclasts type-σ Clockwise rotation	Fracturing SGR BLG Twinning deformation Undulose extinction Pertites flame	GBM, SGR	≈ 450 - 500

BLG: bulging; SGR: subgrain rotation; GBM: grain boundary migration

Table 3. Grains statistics from recrystallized quartz analyzed using PolyLX *toolbox* in MATLAB.

Samples	Number of grains	Area (µm²)		Roundness (%)		Long axis orientation (degrees)		Axial ratio		Feret Diameter (µm)		Paris Factor (%)	
		Mean	Sd	Mean	Sd	Mean	Sd	Mean	Sd	Mean	Sd	Mean	Sd
PS-40A	301	1530.44	2345.29	86.38	11.25	10.00	30.28	1.63	0.35	52.46	23.16	5.84	3.90
PS-40D	244	3856.19	2855.76	50.56	11.44	18.73	23.02	1.73	0.36	62.79	24.27	4.86	3.38
PS-41A	258	2113.41	1512.88	52.40	10.29	12.68	30.09	1.67	0.38	46.73	17.64	6.39	3.88
PS-41C	251	4947.67	4497.72	52.34	11.34	12.93	31.42	1.69	0.35	66.40	32.20	4.55	3.10
PSB-05B	309	2664.50	1887.42	56.91	10.83	16.00	33.18	1.54	0.28	52.35	20.00	3.53	2.44
PSB-06	299	1703.92	1184.86	57.15	10.98	9.66	37.44	1.52	0.28	42.12	15.73	3.64	2.71
PSB-08	232	3727.17	3425.63	56.63	10.12	9.63	40.13	1.51	0.27	57.54	26.31	5.62	3.49
PSB-09	271	2594.75	2156.00	56.02	10.41	1.00	32.63	1.53	0.27	50.17	21.85	5.18	3.90

Table 4. Vorticity results calculated using rigid porphyroclast (W^{RP}_m) and δ/β ($W^{\delta/\beta}_m$) methods.

Sample		Rigid Porphyroclast method				δ/β method		
		R_c min	R_c max	W^{RP}_m min	W^{RP}_m max	δ(°)	β(°)	$W^{\delta/\beta}_m$
NE Sector	PS-40A	-	-	-	-	20	10	0.86
	PS-40B	2.0	2.3	0.60	0.68	-	7	-
	PS-40D	-	-	-	-	19	10	0.85
	PS-41A	1.8	2.4	0.53	0.70	13	1	0.40
	PS-41B	1.9	2.3	0.56	0.68	-	11	-
	PS-41C	1.7	2.1	0.48	0.63	13	7	0.64
	PS-42A	-	-	-	-	-	5	-
	PS-42B	1.8	2.2	0.52	0.65	-	14	-
Central sector	PS-55	1.7	2.3	0.48	0.68	-	29	-
	PSB-05B	-	-	-	-	16	28	0.99
	PSB-06	-	-	-	-	20	10	0.87
	PSB-08	1.6	2.3	0.43	0.68	9	5	0.47
	PSB-09	1.65	2.1	0.46	0.63	1	6	0.24

Table 5. Paleopiezometry based on diameter of quartz grains recrystallized during mylonitization process.

Samples	Number of grains	Feret diameter (μm)	Piezometry (Stipp and Tullis, 2003)	Error	Piezometry (Twiss, 1997)
		Mean	MPa	(%)	MPa
PS-40A	301	52.46	28.44	14.62	41.63
PS-40D	244	62.79	25.03	16.10	36.84
PS-41A	258	46.73	31.65	13.68	45.04
PS-41C	251	66.40	23.95	16.53	35.46
PSB-05B	309	52.35	28.49	14.63	41.70
PSB-06	299	42.12	34.37	12.86	48.34
PSB-08	232	57.54	26.83	15.39	39.01
PSB-09	271	50.17	29.91	8.51	42.91